Feasibility study of power generation through waste heat recovery of wood burning stove using the ORC technology

Rahbar, Kiyarash; Mahmoud, Saad; Al-Dadah, Raya; Moazami, Nima; Ashmore, David

DOI:
10.1016/j.scs.2017.09.013

Document Version
Peer reviewed version

Citation for published version (Harvard):
Rahbar, K, Mahmoud, S, Al-dadah, RK, Moazami, N & Ashmore, D 2017, 'Feasibility study of power generation through waste heat recovery of wood burning stove using the ORC technology', Sustainable Cities and Society, vol. 35, pp. 594-614. https://doi.org/10.1016/j.scs.2017.09.013

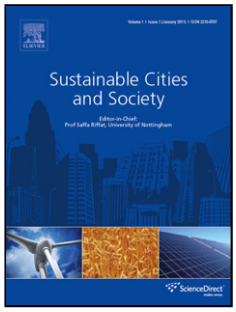

Title: Feasibility study of power generation through waste heat recovery of wood burning stove using the ORC technology

Authors: Kiyarash Rahbar, Saad Mahmoud, Raya K. Al-Dadah, Nima Moazami, David Ashmore

PII: S2210-6707(17)30242-1
DOI: http://dx.doi.org/10.1016/j.scs.2017.09.013
Reference: SCS 767

To appear in:

Received date: 6-3-2017
Revised date: 7-8-2017
Accepted date: 10-9-2017

Please cite this article as: Rahbar, Kiyarash., Mahmoud, Saad., Al-Dadah, Raya K., Moazami, Nima., & Ashmore, David., Feasibility study of power generation through waste heat recovery of wood burning stove using the ORC technology.*Sustainable Cities and Society* http://dx.doi.org/10.1016/j.scs.2017.09.013

Feasibility study of power generation through waste heat recovery of wood burning stove using the ORC technology

Kiyarash Rahbar[a]*, Saad Mahmoud[a], Raya K. Al-Dadah[a], Nima Moazami[a], David Ashmore[b]

[a] School of Mechanical Engineering, University of Birmingham, Edgbaston, Birmingham B15-2TT, UK

[b] Landy Vent UK Ltd, 2 Redditch road, Studley, Warwickshire, B80-7AX, UK

Highlights

- Various strategies to minimize heat losses of Biomass stove by implementing an ORC system was investigated.
- Stove's temperature distribution and potential location for evaporator were obtained using experimental testing.
- "Modification 2" was the most effective which improves stove's efficiency by about 20% while generating 1.113kW of electricity.

Abstract:

Waste heat recovery of low-to-medium grade heat sources such as solar energy or biomass using Organic Rankine Cycle (ORC) technology has received growing attention recently. Few manufacturer of biomass (wood logs) stoves utilizes silicon-carbide as the material for manufacturing of their stoves to facilitate slow-heat-release for a long period of time for up to twelve hours. Despite good performance of these stoves, there is still significant amount of heat that is wasted through exhaust at the temperature of between 240°C to 270°C. This paper investigated various strategies to minimize heat losses to the environment by introducing an ORC system that can capture the waste heat and convert it into useful power. The stove's temperature distribution as well as identification of potential location for the ORC evaporator were obtained using experimental testing. Such results were then employed for validation of a CFD model and it was shown that this CFD model can fairly accurately predict both temperature distribution and recovered heat on the ORC evaporator coils. Among investigated scenarios, "Modification 2" proved to be most effective as it not only preserved the heating functionality of the stove but also improved the stove's efficiency by about 20% while generating 1.113 kW of electricity.

Keywords: Organic Rankine Cycle; waste heat recovery; CFD; Conjugate heat transfer; biomass; thermal analysis

*Corresponding author. Tel.: +44(0)1214143513. E-mail addresses: kxr965@alumni.bham.ac.uk, kiyarash.rahbar@gmail.com

1. Introduction

Following the International Energy Agency (IEA) report [1], extending the current trend of energy consumption and energy efficiency to 2050 yields in a growth of 70% and 60% in the global energy demands and emissions respectively compared to 2011. The associated emissions result in a long-term global average temperature rise of 6 °C by 2050 which can result in potentially devastating consequences such as climate change, energy security and unsustainable future. IEA [1] suggested an effective scenario called "2DS" which offers a vision of a sustainable energy system of reduced gas and carbon dioxide (CO_2) emissions which maintains the global temperature rise within 2 °C by 2050. Improvements in energy efficiency have the major contribution to the "2DS" scenario. For example, power in the traditional electrical grid (or Centralized Power Generation- CPG) followed one way from the generation station to the load. The traditional grid uses the highest possible voltage level to transmit and distribute large quantities of power. During this transport there are associated losses that accounts for 12% of power and 30% of delivered electricity cost as reported by [2]. In addition, there are implicit costs in terms of carbon emissions in which the fuel that is consumed to generate electricity is not fully used by the end user. Therefore, it is necessary to minimize these losses in order to increase the energy efficiency of the system. Moreover, CPG requires large capital investment cost for electrification of remote areas where the infrastructure requires the electricity but at low quantities. Besides, CPG suffers from high cost of electricity deregulation and control devices and harmful environmental impacts due to the use of fossil fuels. In this regard, Distributed (on-site) Power Generation (DPG) is a promising alternative that overcomes all the deficiencies of the CPG. DPG is an independent electric source

connected directly to the distribution network or to the customer site with the power ratings shown in Table 1 [3].

Table 1 Power rating of the DPG systems [3]

Category	**Power rating**
Distributed micro power generation	1Watt to 5kW
Distributed small power generation	5kW to 5MW
Distributed medium power generation	5MW to 50MW
Distributed large power generation	50MW to 300MW

DPG is becoming a new trend in the world's ever-increasing demand for energy as it exhibits unique advantages such as reduced transmission and distribution losses, emergency backup power in the case of power outage for hospitals, telecommunications centres, domestic markets, office buildings, schools, leisure centres and farms, environmentally friendlier than CPG, versatility for suppling the power demand into remote areas (i.e. farms) and security and reliability due to its compatibility with wide range of fuels. In fact DPG can utilise any source of energy or waste heat.

About 50% of the world's energy consumption is wasted as heat due to the limitations of energy conversion processes [4]. This waste heat can be from variety of sources such as industrial and household waste heat, solar radiation, geothermal heat and biomass heat. Adopting the Waste Heat Recovery (WHR) with Distributed Power Generation (DPG) systems has a great potential in increasing the system efficiency while reducing the fuel consumption and lowering the CO_2 emissions with enhanced substantiality [4]. In this regard, biomass heat has received growing attention for WHR systems in the past few years. Biomass is the world's fourth largest energy source providing about 10% of the world's energy demand [5]. Biomass is widely available from several industrial and agricultural processes such as furniture industry or agricultural and forest residues. Biomass has great potential in providing Combined Heat and Power (CHP) simultaneously. Biomass can be transformed into heat using combustion and

the heat can be converted into electricity using the Organic Rankine Cycle (ORC). ORC is one of the most reliable technologies that can convert this otherwise wasted heat into useful electricity with unique features such as simple structure, low maintenance and cost, small size and high efficiency if the heat source temperature is below 350 ˚C [6].

Few manufacturers of biomass (wood logs) stoves such as [7] utilize silicon-carbide as the material for manufacturing of their stoves. With high thermal capacity of silicon-carbide such stoves perform better the conventional metallic ones where they can work as a heat storage system and retain the thermal energy for a long period (up to twelve hours) and then release it slowly for space heating [8]. Despite the good performance of these stoves, there is still significant amount of energy loss (about 40%) in the form of waste heat through the exhaust at the temperature of around 240 ˚C to 270 ˚C [8]. Therefore, there is a need to enhance the performance of these stoves by introducing a WHR system that can capture substantial amount of this waste heat and convert it into useful power and thus improving the overall energy efficiency, reducing carbon emissions and increasing the stove's market penetration.

Few studies were conducted in the literature that mainly investigated the CFD modelling of the wood burning biomass stoves or the optimization of the stove geometry for improving the performance. Dixon *et al.* [9] demonstrated the importance of the CFD tool in simulating the biomass combustion and highlighted the summary of the applications that showed the successful implementation of the CFD. Ravi *et al.* [10] presented an approach in which detailed CFD simulations of the flow, heat transfer and combustion in a simple sawdust stove were used to evolve simple algebraic equations that describe individual phenomena. They eventually showed the development of building blocks from detailed simulation and their use in derivation of simple equations relating the design and performance. Scharler *et al.* [11] demonstrated the applications and advantages of CFD simulations for the furnaces, wood log fired stoves and boilers. The results showed that the CFD-aided technology led to reduced emissions, better

utilization of the furnace volume and increased flexibility and efficiency of biomass plants. Macqueron [12] studied the thermal and fluid dynamics of a sauna heated by a wood burning stove using NIST's Fire Dynamics Simulator (FDS) software. The simulations were performed in order to obtain the temperature distribution, velocity field, heat flux, soot and steam cloud across the sauna and highlighted the flexibility of the tool for design optimization and safety analysis (oxygen and carbon monoxide levels). Scharler *et al.* [13] utilized the CFD tool to optimized design of wood log fired stoves with regards to CO emissions, fine particulate emission from incomplete combustion. They developed a novel empirical model for wood log combustion and CFD models for the turbulent and reacting flow. The model was validated with commercial stoves in the market with efficiency of more than 80%.

Despite these studies that considered modelling and optimization of wood burning stoves, there is no published work that investigated the feasibility of electricity generation through WHR by integrating the ORC system with biomass stoves. Therefore, this paper aims to investigate the feasibility of this concept by assessing the amount of electricity generation and overall efficiency improvement of a commercially available biomass stove. Experimental testing of the stove will be carried out for evaluating the characteristics of the waste heat as well as obtaining the stove's temperature distribution while identifying the potential position for the ORC evaporator. Moreover, numerical modelling of such stove will be conducted using CFD simulations with conjugate heat transfer to first validate the model as a benchmarking tool and then investigate various modifications to the stove that can enhance the WHR and eventually increase the electricity generation.

2. Organic Rankine Cycle (ORC) structure and modelling

The ORC is similar to the Steam Rankine Cycle (SRC) but instead of water it utilizes organic compounds such as hydrocarbons and/or refrigerants that boil at low temperature and pressure. This facilitates the ultimate versatility of the ORC to capture almost any low to

medium temperature (from 60 °C up to 350 °C) heat sources to generate power. Compared to the SRC, the ORC exhibits unique advantages such as small size, low capital and maintenance cost, simplicity and high reliability when combined with renewables such as biomass, solar energy or geothermal heat. The ORC system consists of four main components as evaporator, condenser, pump and expander as shown in Figure 1. The corresponding temperature-entropy diagram of the ORC is shown in Figure 2 [14].

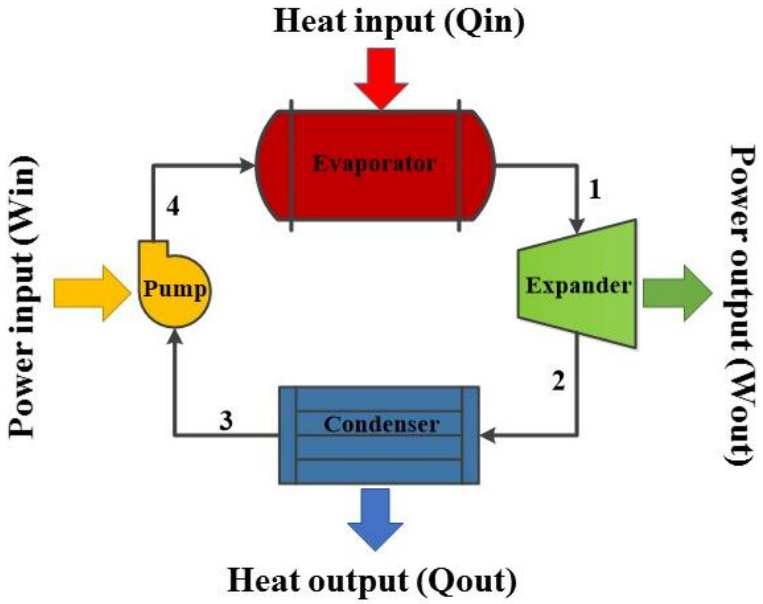

Figure 1 Schematic of Organic Rankine Cycle (ORC) components

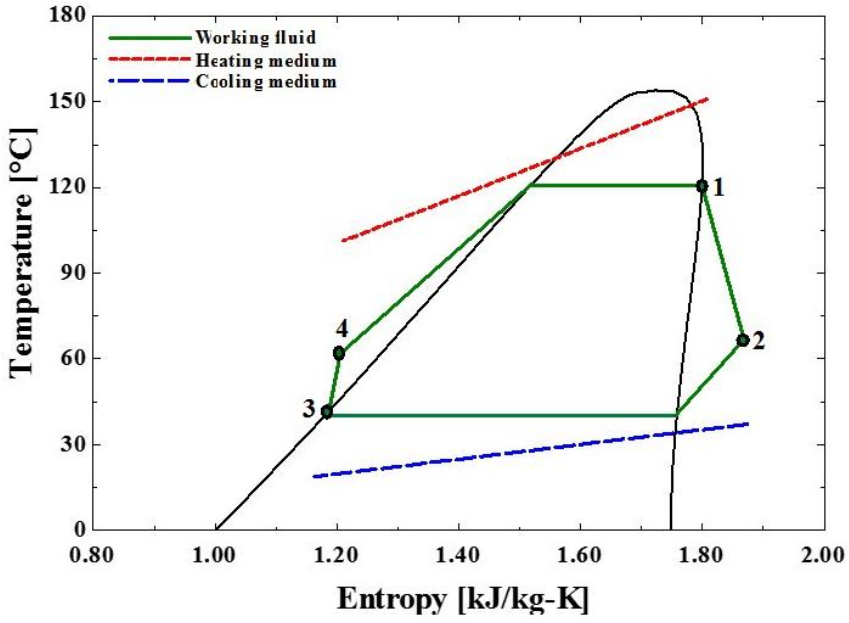

Figure 2 Temperature-entropy diagram of the ORC

Detailed modelling and explanation of different ORC components can be found in [15, 16] and here only the ORC thermal efficiency ($\eta_{thermal,ORC}$) is presented.

$$\eta_{thermal,ORC} = \frac{W_{out}}{Q_{in}} \quad \text{Equation 1}$$

Where $\eta_{thermal,ORC}$ is the ORC thermal efficiency, W_{out} is the net power output from the ORC and Q_{in} is the heat input to the system. Pump power consumption (W_{in}) is normally low and for this study is considered negligible following [17] .

One of the aims of this study is to identify the potential location within the stove under investigation so that the ORC evaporator can be installed for capturing the waste heat (Q_{in}) and then based on the estimation of $\eta_{thermal,ORC}$ the net electricity (W_{out}) can be obtained using Equation 1. Following [18], the maximum obtainable ORC thermal efficiency ($\eta_{thermal,ORC}$) can be determined from Equation 2.

$$\eta_{thermal,ORC} = -14.92 + 0.07339T_{hs,in} + 0.08363T_{hs,out} + 0.1464\eta_{exp} \quad \text{Equation 2-a}$$

$$for\ \ 80\ ^{\circ}\text{C} < T_{hs,in} < 180\ ^{\circ}\text{C}$$

$$\eta_{thermal,ORC} = -12.33 + 0.05858T_{hs,in} + 0.0335T_{hs,out} + 0.2666\eta_{exp} - 0.1552T_c - 0.0810\Delta T_{pp} \quad \text{Equation 2-b}$$

$$for\ \ 180\ ^{\circ}\text{C} < T_{hs,in} < 360\ ^{\circ}\text{C}$$

Where, $T_{hs,in}$ and $T_{hs,out}$ are the heat source inlet and outlet temperatures respectively, T_c is the condenser temperature, ΔT_{pp} is the pinch point temperature difference in the evaporator and η_{exp} is the expander efficiency. All the temperatures are in degree Celsius and the efficiencies are in percent. In this paper T_c, η_{exp} and ΔT_{pp} were kept constant with the values listed in the Table 2.

Table 2 ORC constant parameters

Parameter	Value
Condenser temperature (T_c)	30 °C
Expander efficiency (η_{exp})	75 %
Pinch point temperature difference in evaporator (ΔT_{pp})	10 °C

3. Stove architecture

In this study a commercially available biomass wood burning stove was employed [19]. Such stove can gently warm the area of a three to four bedroom house to a maximum of 240m^2 without overheating the room in which it stands with the temperature in the range of 22 °C to 27 °C [8, 20]. Figure 3 presents the employed stove components and the terminology of different parts such as the "Hotbox", "Top", "Side walls", "Grate", "Bottom" and "Back panel" (yellow colour in the 3-D CAD model) as well as the stove's dimensions. All these parts are manufactured with Silicon-Carbide and further details regarding the stove dimensions and specifications can be found in [8]. It should be mentioned that the stove exhausted to the outside air (the exhaust pipe continued to the outside environment however not shown in Figure 3).

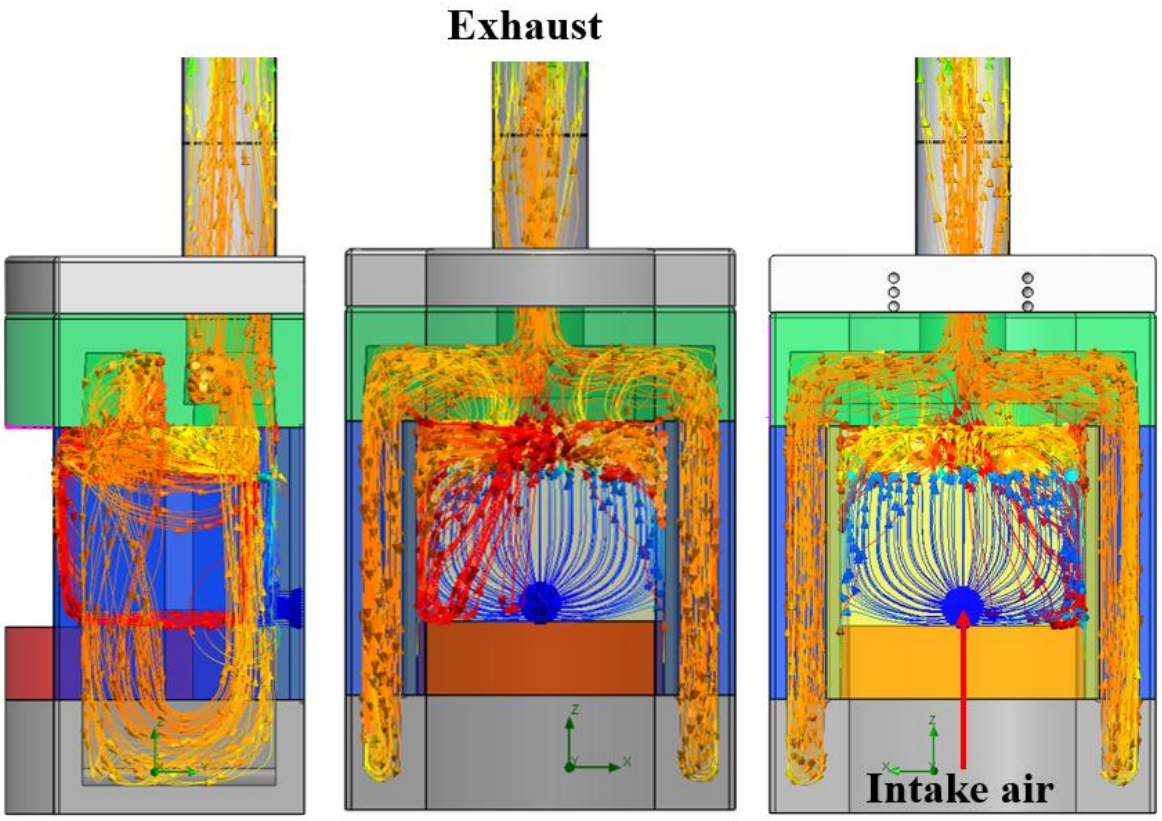

Figure 4 Primary air moving path inside the stove

The primary combustion air enters the stove from the hole at the “Back panel” and reacts with the burning wood. Then it exhausts through the “Top” part and divides into two primary streams in the side channels and then re-merges in the “Top” part again and exits from the exhaust pipe to the surrounding as depicted in Figure 4.

4. Experimental testing of the biomass stove

4.1 Measurement of temperature and flow rate

For characterising the waste heat from the stove and also identifying the potential position for the ORC evaporator, experimental testing of the stove was carried out. Experiments were initially conducted to obtain the temperature distribution so for such purpose the complete stove body was instrumented with thermocouples that were soldered/bonded at various positions illustrated in Figure 5. T_1 was installed at the “Grate” middle, T_2 at the “Grate” edge, T_3 at the “Top” front, T_4 at the “Hotbox” bottom, T_5 at the “Hotbox” top, T_6 in the “Side wall” interior

channel and T_7 at the stove's exhaust pipe. All the thermocouples were T-type Omega TJC100-CPSS-M075G-150 [21] probes with the sheath diameter of 0.75mm and length of 150mm with the maximum temperature limit and accuracy of 316 °C and $\pm$0.5 °C respectively according to the manufacturer [21].

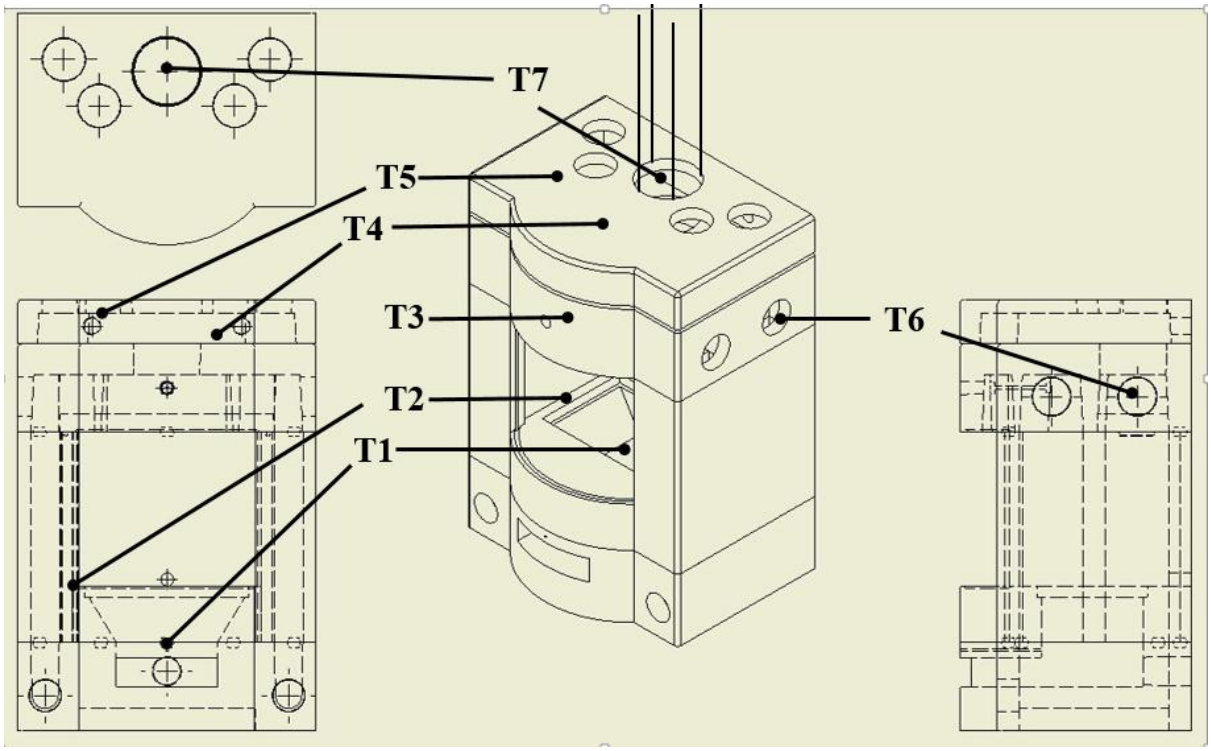

Figure 5 Schematic of the thermocouples' installation positions

All thermocouples were connected to the data acquisition device called Pico TC-08 data logger [22] which was connected to a PC for continuous monitoring and logging of temperature across the stove. Mass flow rate of the flue gasses was measured with a mechanical rotating vane anemometer meter model "Flomaster anemometer" manufactured by "Phoenix Abboflex & instruments Ltd" with the range of up to 15m/s and was installed in the exhaust pipe near T_7 thermocouple and insulated with glass wool. The flow meter measured the velocity of the flue gases and the mass flow rate was calculated using Equation 3.

$$\dot{m} = \rho V A_{exhuast\ pipe} \quad \text{Equation 3}$$

Where ρ is the air density (kg/m^3), V is the flow velocity (m/s) measured by the flow meter and $A_{exhust,pipe}$ is the area of the exhaust pipe (m^2) known from the geometry of the stove. A pressure tapping hole was fitted next to the flow meter on the exhaust pipe and was connected with stainless steel insulted pipe to a manometer for measuring the flue gas exhaust pressure. With the known exhaust temperature (T_7) and pressure the density (ρ) was obtained using Engineering Equation Solver (EES) reliable thermodynamic property functions and $\dot{m}$ was calculated. Although, it was easier to measure the flow velocity at the cold intake instead of the procedure outlined above, due to technical difficulties of flow meter installation and requirements of modifications at the inlet of stove, it was decided to measure the flow velocity and therefore the mass flow rate at exhaust of the stove.

The investigated stove can take up to 13kg of wood in its combustion chamber. The wood logs used in all experiments were "Silver Birch" with the characteristics shown in Table 3.

Table 3 Properties of the Silver Birch wood [23]

Parameter	Value
Density	640 (kg/m^3)
Thermal conductivity	0.15 (W/m-K)
Specific heat	2000 (J/kg-K)
Energy content	4.2 (kWh/kg)

Temperatures were logged and the results are shown in Figure 6. Obviously, the highest temperature was achieved in the "Side wall" interior channel with the value of 354 ˚C averaged over to 13000s while the lowest temperature was recorded for the "Grate" with the value of 105 ˚C averaged between the "Grate" edge and "Grate" middle. Table 4 summarizes the average temperatures in a ranking order at various positions in the stove.

Table 4 Ranking of the temperature measurement positions for burning 12.9kg of wood

Rank	Position	Average temperature up to 13000s
1	Side wall	354.3 ˚C
2	Top front	344.8 ˚C
3	Exhaust	272.9 ˚C
4	Hotbox	192.6 ˚C

5	Grate	104.9 ˚C

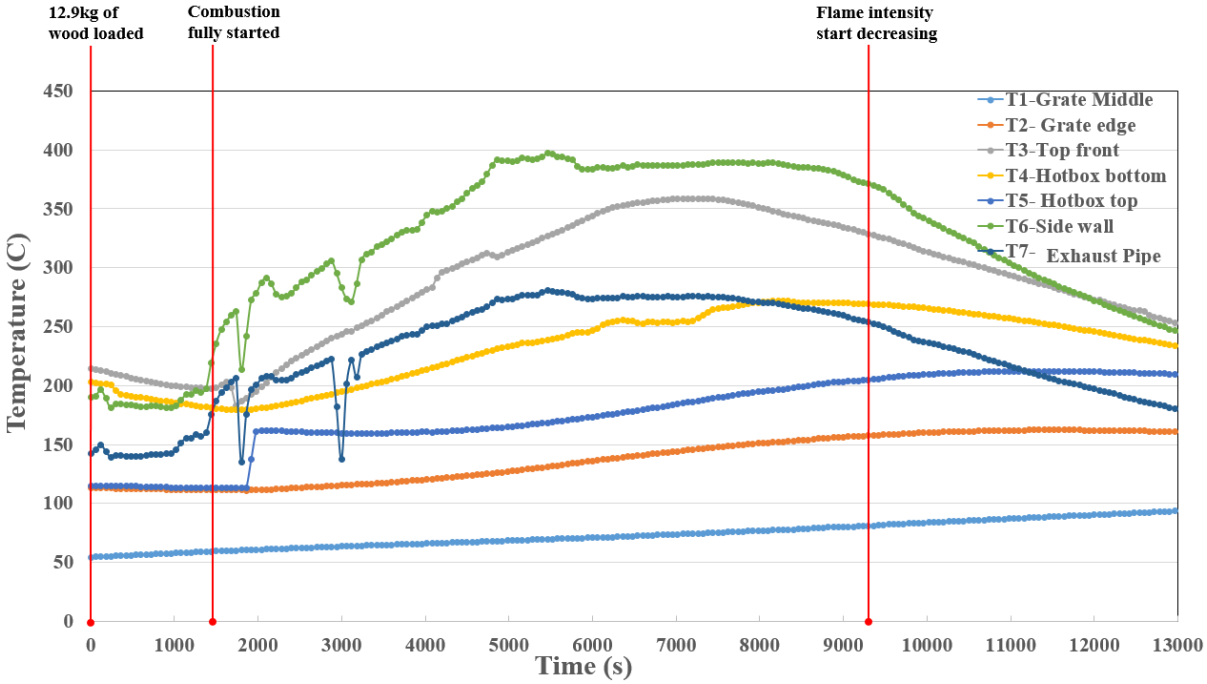

Figure 6 Temperature distribution across the stove while burning total of 12.9kg “Silver Birch” wood logs

Moreover, Figure 6 shows that the stove can generate steady temperature for a significant amount of time (from 5000s to 9000s) and the heat can be continuously supplied with minimal variation and at highest possible temperature suitable for WHR. The mass flow rate measurement of flue gases using Equation 3 resulted in the flow rate variation of between 0.0134 kg/s to 0.0284 kg/s at the start and peak of combustion process respectively.

4.2 Measurement of waste heat power

Following the temperature and flow rate measurements, it was required to measure the waste heat power from the stove. Such measurements were obtained by fabricating a closed loop water heating system with heating coils (i.e. ORC evaporator) inside the stove and measuring the temperature rise. However, the position of the heating coils was critical to maximize the exposed heat on the heating coils while satisfying the following criteria:

- High temperature

- Physically suitable to accommodate heating coils with minimal effect on the primary functionality of the stove which is heating.
- Requires minimal alteration/modification of stove to install the heating coils (low cost)

It was clear from the results in Figure 6 that, "Side wall" and "Top" parts were the most promising positions in terms of temperature, however, installation of the ORC evaporator in the form of coils inside the "Side wall" channels could cause the flow blockage due to the significant amount of ashes that forms during combustion and could result in back pressure inside the stove combustion chamber leading to smoke leakage into the room. On the other hand, the "Top" part was a solid block with no available space to install the ORC evaporator coils and it required new casting process which was prohibitive in terms of cost and complexity. However, the investigated model has pre-fabricated voids within the "Hotbox" and "Grate" parts as illustrated in Figure 7. Such voids were used to accommodate the ORC evaporator coils with minimal alteration to the stove.

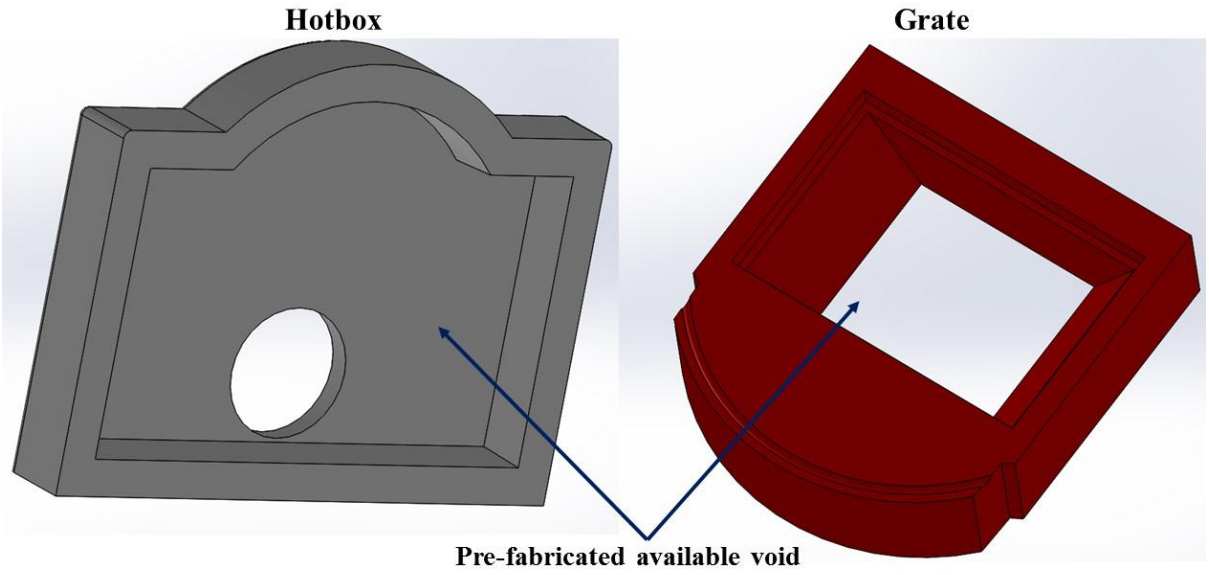

Figure 7 Pre-fabricated void space within the "Hotbox" and "Grate"

The closed loop water heating system was integrated with the stove which included stainless steel ORC evaporator coils, water circulation pumps, water flow meter, one

thermocouple (T-type Omega TJC100-CPSS-M075G-150) at water inlet to the stove and one at the water outlet from the stove. It should be noted that the water circulation pumps are different from the organic feed pump that shall be used in the original ORC systems. In this experimental approach the main aim is to measure the waste heat that is available for the purpose of waste heat recovery with the ORC by using a water circulation and for validation purposes. Both the "Hotbox" and "Grate" voids were completely filled with the stainless steel coils with the total length of 48m (24m in each), inner diameter of 10mm and outer diameter of 18mm. Such coils were then casted by pouring Silicon-Carbide to thoroughly fill the void. Figure 8 shows the detailed casting procedure of the coils in the "Grate" part.

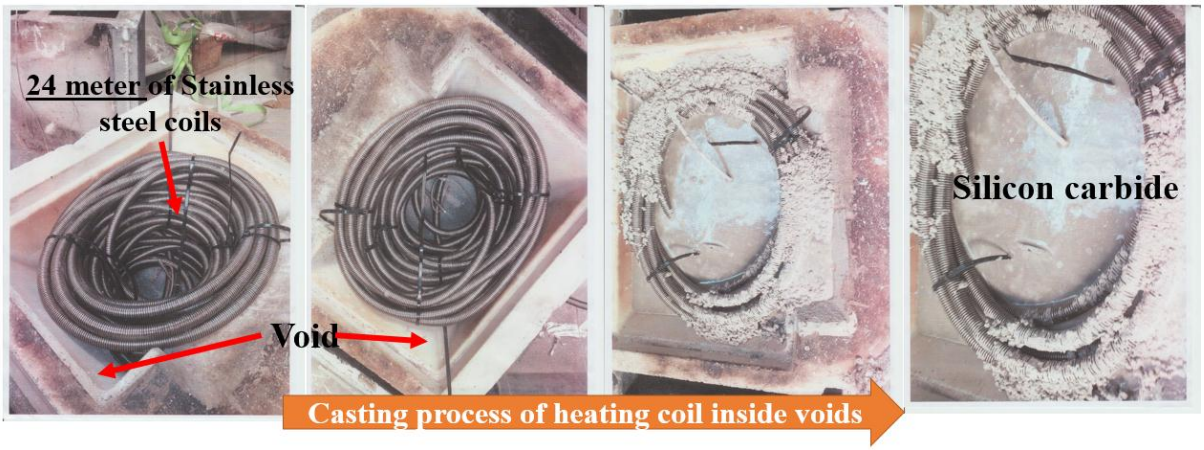

Figure 8 The casting procedure of the heating coils inside the "Grate" cavity

The fabricated experimental facility integrated with the stove and the schematic of the coils and water circuit are shown in Figure 9. The cold water was pumped from the storage tank and entered the stove in the "Hotbox" section. Then it passed through the coils casted in the "Hotbox" while its temperature increased by capturing the heat. The heated water then discharged from the "Hotbox" and transferred with pipes to the "Grate" section where it again circulated through the coils for further increase of temperature. The fully heated water circulated back to the storage tank with the pumps and the process was repeated. With the

measured water flow rate and water inlet and water outlet temperatures the amount of the heat exposed on the stainless steel coils (ORC evaporator) was determined using Equation 4.

$$Q = \dot{m}_{water} C_p (T_{water,out} - T_{water,in}) \quad \text{Equation 4}$$

Where Q(W) is the exposed heat on the coils and C_p is the specific heat capacity (J/kg-K) that was obtained at the average temperature between the water inlet and outlet.

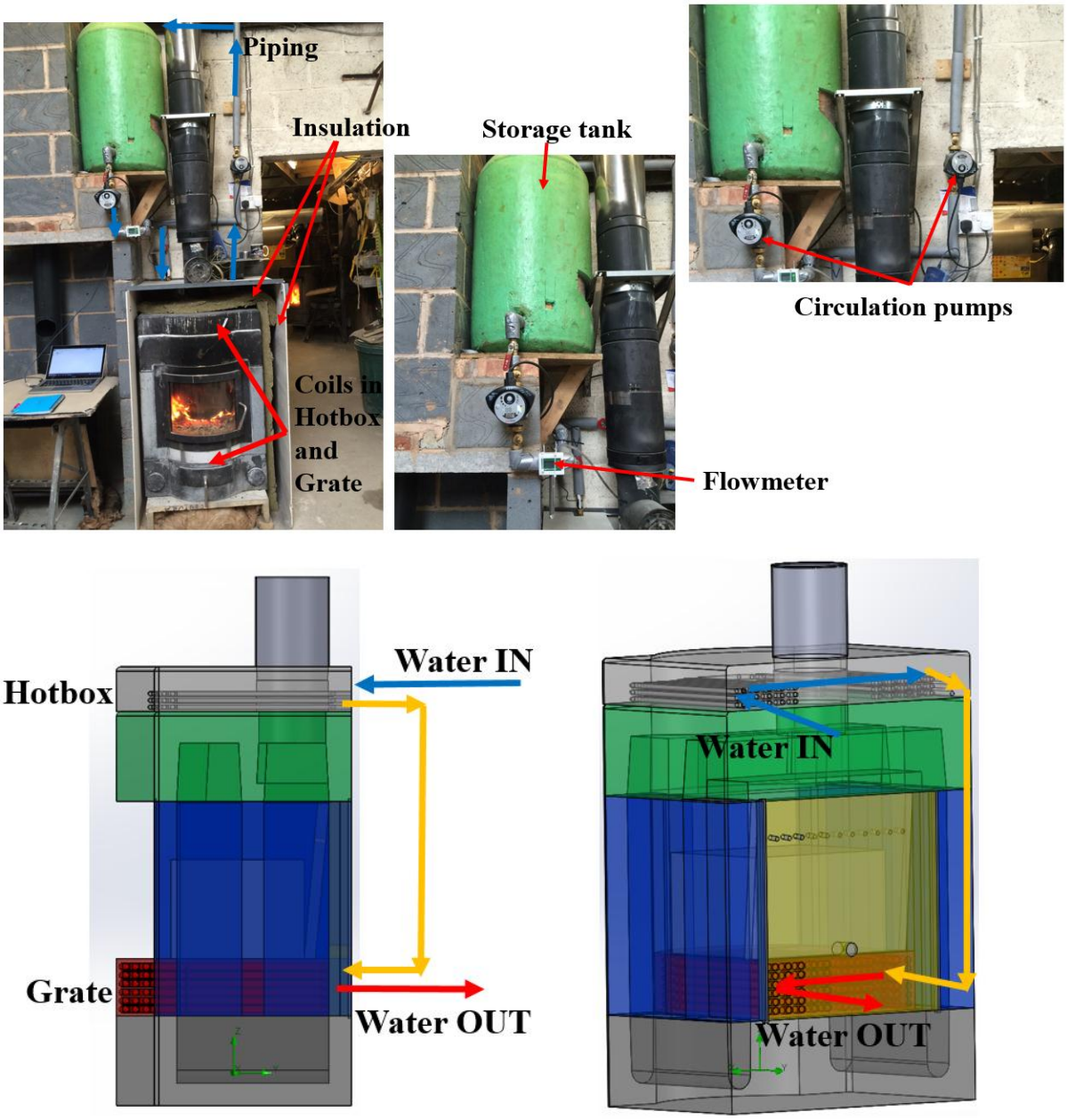

Figure 9 Experimental test setup (top) and schematic (bottom) of the closed loop water heating system configuration in the "Hotbox" and "Grate" parts

The circulating pumps were model "INP0117-INP130-25-5a" manufactured by "Interpart Ltd" with the maximum head of 15m and maximum flow rate of 2.8m^3/hr [24]. The water flow meter was model "DigiFlow 6710M" manufactured by "Futurlec Ltd" with the maximum flow rate of 25 lit/min [25]. Similar to section 4.1, about 13.2kg of "Silver Birch" wood was burned and the results are presented in Figures 10 and 11.

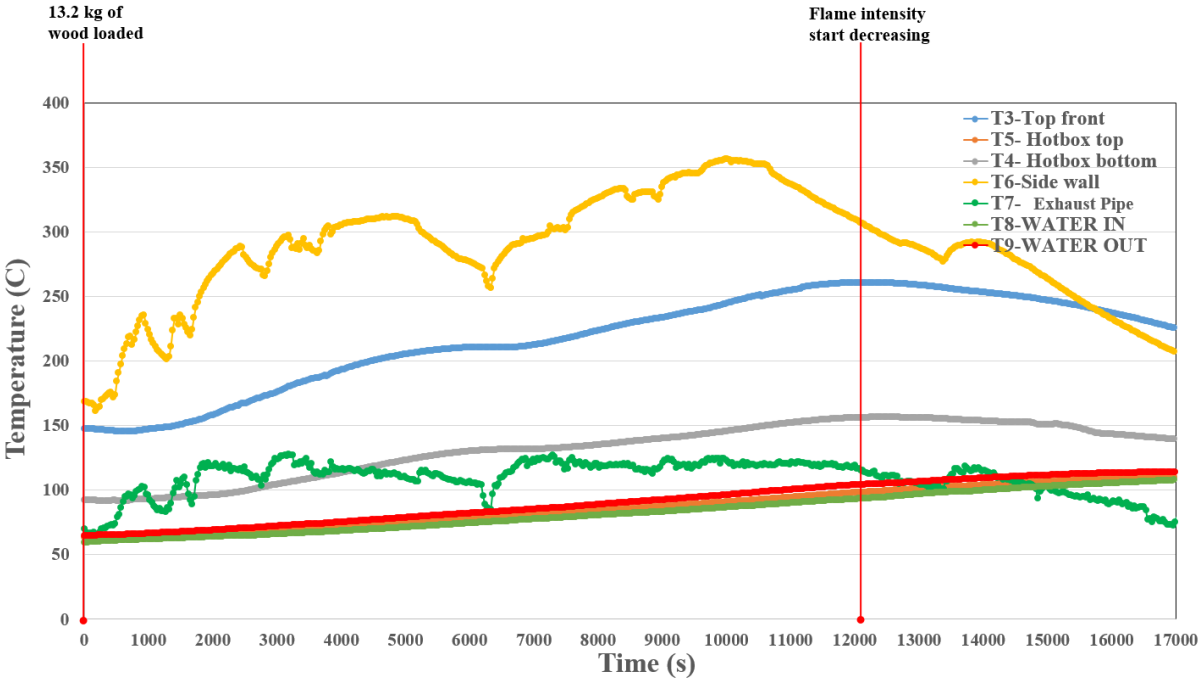

Figure 10 Temperature distribution across the stove with water heating system (burning 13.2kg wood)

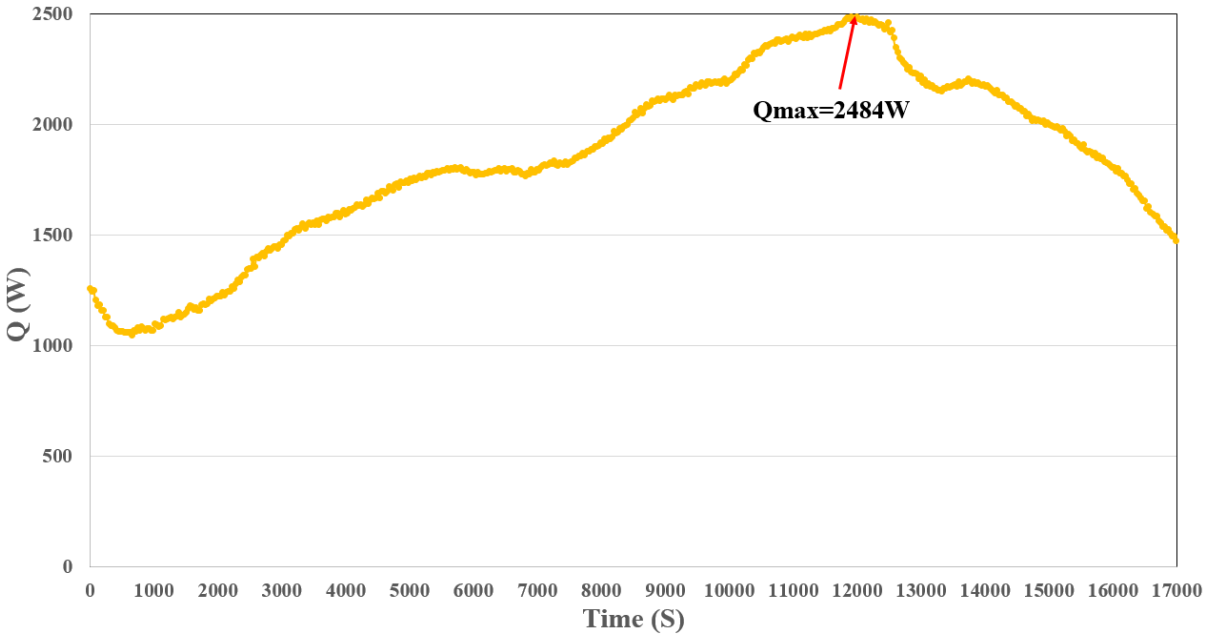

Figure 11 Calculated exposed heat on the ORC evaporator coils with the water heating system (burning 13.2kg wood)

It is clear from Figure 10 that the ranking order of the hot spot positions remains the similar to Figure 6 with the maximum temperature achieved in the "Side wall" interior channels. Table 5 summarizes the average temperature at various measurement points.

Table 5 Ranking of the temperature measurement positions for water heating system (burning 13.2kg of wood)

Rank	Position	Average temperature up to 17000s
1	Side wall	283.1 ˚C
2	Front Top	217.8 ˚C
3	Exhaust	110.3 ˚C
4	Hotbox	109.5 ˚C
5	Grate	68.1 ˚C

Comparing the results of the average temperature of "Hotbox" in Tables 4 and 5 reveals that the "Hotbox" temperature has reduced significantly by about 83.1 ˚C. This is due to the fact that the heat exposed to the "Hotbox" was absorbed by the coils to increase the water temperature leading to reduction of the "Hotbox" temperature. Using the measured water flow rate shown in Figure 12 together with Equation 4, the maximum heat (Q_{in}) of 2484W was captured by the coils at about 12000s as depicted in Figure 11. Since the volume flow rate is measured by the flowmeter and its recorded values are shown in figure 12, the corresponding mass flow rate obtained by equation 3 is also overplayed in the same figure for the exact values

used in the analysis. Such value is equivalent to about 13.7% of the total heat dissipated by the stove (18.2kW) as will be shown in section 5.1 below.

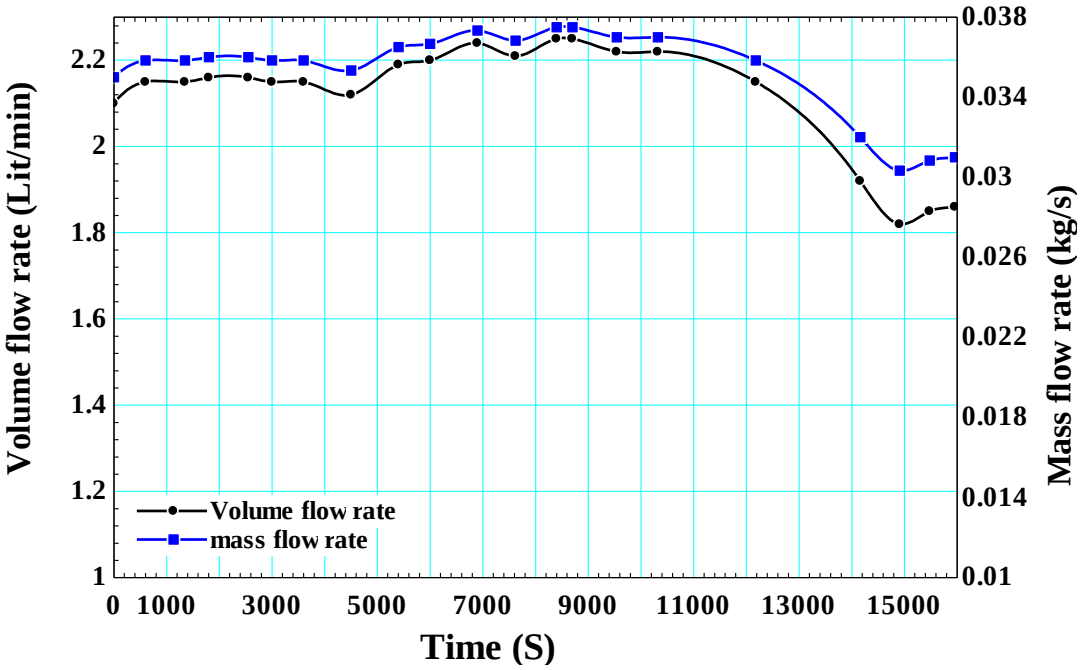

Figure 12 Measured volume and mass flow rate for the water heating system (burning 13kg of wood)

In order to estimate $\eta_{thermal,ORC}$ using Equation 2, it was required to determine the heat source inlet and exit temperatures ($T_{hs,in}$ and $T_{hs,out}$). Since in this study the heat source is the stove solid body heat, the heat source inlet temperature ($T_{hs,in}$) was considered to be the average of the "Hotbox" and "Grate" solid temperatures before implementing the water heating system (i.e. the values in Table 4) while the heat source outlet temperature ($T_{hs,out}$) was considered to be the average of the "Hotbox" and "Grate" parts after implementing the water heating system (i.e. the values in Table 5). Hence, based on such assumption, $T_{hs,in}$ and $T_{hs,out}$ of 148.8 ˚C and 88.8 ˚C were achieved respectively. Utilizing Equation 2-a (as $T_{hs,out}$ was less than 180 ˚C) and the default values for the rest of constants (Table 2), led to $\eta_{thermal,ORC}$ of 14.4%. With the calculated $Q_{in,max}$ of 2484W (Figure 11) and Equation 1, the maximum net electricity output of 357.7W can be achieved if the ORC system is integrated with the stove with its evaporator located in the "Hotbox" and "Grate" parts. Although the generated power is low for such

experimental setup, this experiment serve as basis for validation of the CFD model in the following sections as well as investigating various scenarios to further increase the power output of the ORC system integrated with the biomass stove.

5. Numerical CFD and thermal simulation of the stove

Following the stove experimental testing, it was required to perform CFD simulations to initially validate the developed CFD model and then employ that as a benchmark model to further investigate various modifications of the ORC evaporator coils for further increasing the net electricity generation. The CFD simulations were conducted using SolidWorks FlowSimulation 2014 package [26]. Such package has great flexibility in terms of CAD modelling with CFD simulations and conjugate heat transfer module all in one reliable and agile platform.

5.1 Simulation physics, CFD and thermal modelling setup and grid generation

The combustion inside the stove includes all the modes of heat transfer as conduction, convection and radiation. The heat from the combustion of wood logs is emitted via radiation to the stove inner walls and to the outside environment through the glass door (Although, the authors agree that general CFD codes such as FlowSimulation are usually unable to accurately calculate the power radiated by flame compared to the more advanced and professional codes such as Fire Dynamics Simulator due to occurrence of flame thermal gradients in very thin layers, it is assumed that the results for this study are preliminary and the discrepancies in the simulated and experimental values are originated from this issue. However, since this study is pioneering in the application of waste heat recovery of biomass stoves with ORC, the proposed methodology and the preliminary results are valuable). Part of the heat is carried by the flue gases through the exhaust while part of the heat is transferred via conduction from the stove inner walls to the stove outer walls and then it both emitted by radiation to the surrounding and by the natural convection to the surrounding environment. All modes of heat transfer were

defined during simulation setup using FlowSimulation package with conjugated heat transfer model that includes both the heat transfer in the solids (conduction) as well as fluids (convection). FlowSimulation utilizes two approaches for modelling the radiation called discrete transfer and discrete ordinate models. The former approximates the radiation leaving the surface element in a certain range of solid angles by a single ray. The radiation heat is transferred along a series of rays emanating from the radiative surfaces only. Rays are then traced as they traverse through the fluid and transparent solid bodies until it hits another radiative surface. This approach, usually called "ray tracing", allows "exchange factors" to be calculated as the fractions of the total radiation energy emitted from one of the radiative surfaces that is intercepted by other radiative surfaces. The latter solves the radiative transfer equation for a finite number of discrete solid angles, each associated with a vector direction. In this study discrete ordinate model has been used as it can model the absorption and/or spectral dependencies as well as capability for absorption of heat radiation in solids in accordance with the specified absorption coefficient which are not available in the other model. Further details of both models can be found in SolidWorks FlowSimulation technical reference guide [26].

The temperature-dependant properties of Silicon-Carbide were defined in the FlowSimulation using the data shown in Figure 13 with the density of 3210 kg/m^3. The glass door was manufactured by “Schott Robax Ltd” and its properties were obtained from the manufacturer [27] . The ORC evaporator coil material was assigned to stainless steel 321 while exhaust pipe was set to aluminium. The biomass wood logs were represented as a single cubic block with the same volume corresponding to the burned mass (13.2kg) and “Silver Birch” properties were assigned to it (Table 3). In addition, based on the energy content of the “Silver Birch” shown in Table 3, the rate of heat release from the wood logs was estimated based on the mass of burned wood logs and the corresponding time recorded from the experiment. 13.2kg of the “Silver Birch” wood logs released 54.6kWh (13.2×4.2) of energy equivalent

to 1.996×10^8J and based on the results in Figure 10 about 3hours were required for such energy to be released resulting in heat generation rate of 18.2kW. Such value was specified to the wood log block to represent the combustion heat generation rate. Although, it is known that the power generated by the wood logs are lower compared to the peak of combustion, it is assumed that the generated power is constant throughout for the simplicity of simulation and also due to the computational cost. Additionally, the stove has the characteristics of slow heat release due to properties of silicon-carbide. This means that after loading the stove with a batch of wood logs, the stove absorb the heat as thermal mass and then release that over a period of 12 hours even after the end of combustion (according to the manufacturer). Therefore, it can be assumed that the stove has a steady-state behaviour in terms of releasing the heat. Therefore, all the numerical simulations in the next section were conducted in the steady state conditions. FlowSimulation utilizes the Favre-averaged Navier-Stokes equations where time-averaged effects of the flow turbulence (turbulence flow was considered for this study) on the flow parameters are considered, whereas the other, i.e. large-scale, time-dependent phenomena are taken into account directly. FlowSimulation employs transport equations for the turbulent kinetic energy and its dissipation rate, the so-called k-ε model. A laminar/turbulent boundary layer model is used to describe flows in near-wall regions. The model is based on the so-called Modified Wall Functions approach. The modified wall function uses a Van Driest's profile instead of a logarithmic profile. If the size of the mesh cell near the wall is more than the boundary layer thickness the integral boundary layer technology is used. FlowSimulation solves the governing equations with a discrete numerical technique based on the finite volume (FV) method. Further details can be found in SolidWorks FlowSimulation technical reference guide [26]. Additionally, only single phase flow has been considered which means that each subdomain will remain in its initial phase during simulation (however, there are two types of fluid which are air and water).

FlowSimulation solves the time-dependent set of equations for all problems, including steady-state cases. For such cases it is necessary to recognize the moment when a steady-state solution is attained and therefore the calculation should be finished. A set of independent finishing conditions offered by FlowSimulation allow the user to select the most appropriate conditions and criteria on when to stop the calculation including convergence of the Goals. The Goals convergence finishing condition is complex since it consists of satisfying all the specified Goals criteria. A specified Goal criterion includes a specified dispersion, which is the difference between the maximum and minimum values of the Goal, and a specified analysis interval over which this difference (i.e., the dispersion) is determined. The interval is taken from the last iteration rearwards and is the same for all specified Goals. The analysis interval is applied after an automatically specified initial calculation period (in travels), and, if refinement of the computational mesh during calculation is enabled, after an automatically or manually specified relaxation period (in travels or in iterations) since the last mesh refinement is reached. As soon as the Goal dispersion obtained in the calculation becomes lower than the specified dispersion, the Goal is considered converged. As soon as all Goals included in the Goals convergence finishing condition (by selecting them in the On/Off column) have converged, this condition is considered satisfied. For this study various global and surface goals at inlet and exit of fluid subdomain were specified including mass flow rate, temperature and pressure. Further details can be found in SolidWorks FlowSimulation technical reference guide [26].

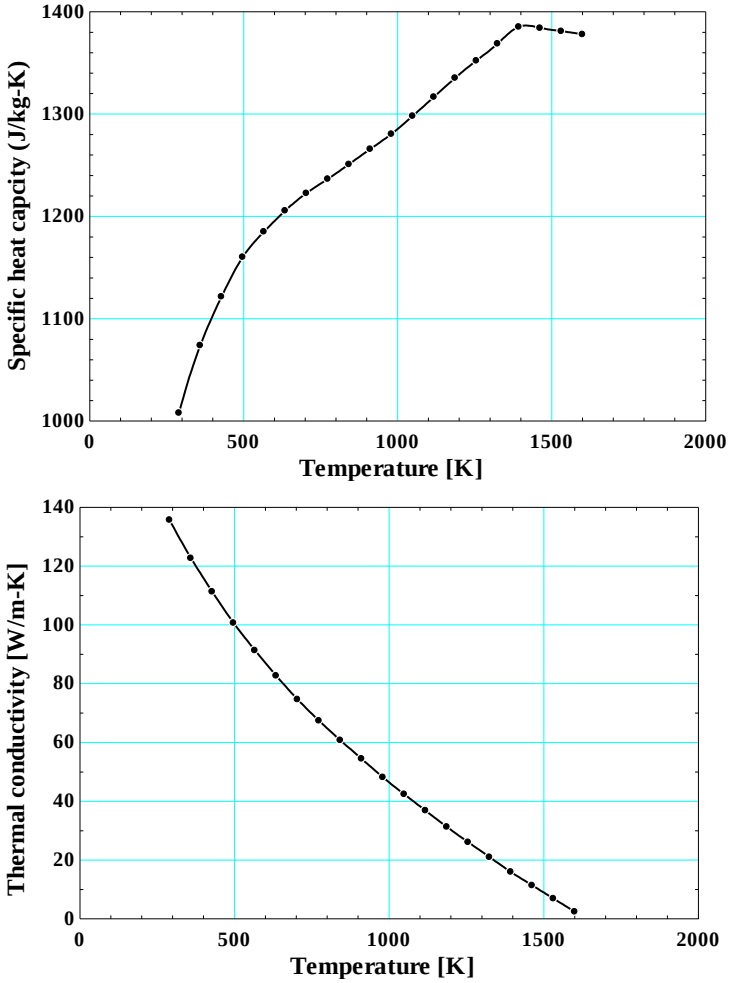

Figure 13 Silicon Carbide temperature-dependent properties

The simulation domain and sub-domain and the associated room dimensions that the experiments were carried out are shown in Figure 14. The room was filled with air and completely isolated from the surrounding. The boundary conditions were specified for the sub-domain (the stove) by specifying the mass flow rate at the inlet of the "Back panel" hole where the air was sucked inside and the environment pressure was specified at the exit of the exhaust pipe (Figure 15). The inlet air temperature to the stove and the initial room temperature were all assigned to 10°C representing the environment temperature in a cold winter day.

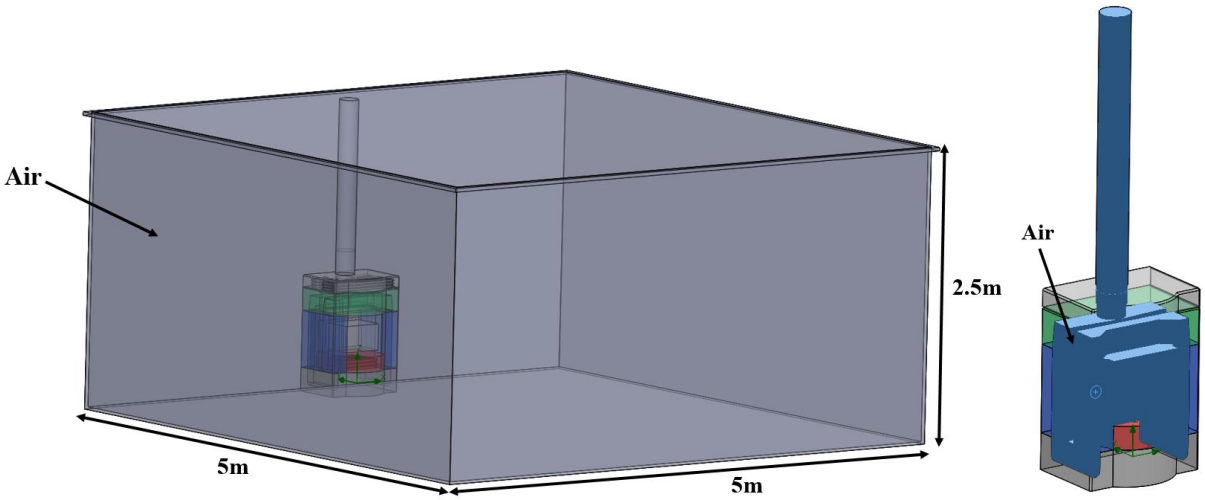

Figure 14 CFD simulation domain (left) and stove sub-domain (right)

In addition, the heat generation rate of 18.2kW was assigned to the cubic wood log block. Figure 15 details the specification of the boundary conditions. The wood log is not only considered as the volume heat source, but also it was considered as a diffusive radiative source (due to its high temperature). Although, it is known that the flame produced by the combustion of wood logs is another source of radiation to the surrounding chamber, inclusion of such phenomena requires more advance simulation techniques such as Fire Dynamics Simulator (FDS) that can lead to much more accurate results. However, it is known that, in very confined volumes the effect of radiation is weakened. Overall, exclusion of this factor is one of the reasons for deviation of numerical and experimental results. All the six faces of the wood log block were assigned as radiative surfaces with emissivity of 0.75. Moreover, both the inner surface of the combustion chamber and the outer surface of the stove was specified as radiative surfaces with the emissivity coefficient of 0.87 for Silicon-Carbide following [28]. Similarly the exhaust aluminium pipe was also considered as a radiative surface with the emissivity coefficient of 0.09 obtained from SolidWorks built-in library for commercial aluminium sheet. Figure 16 details the specification of the radiative surfaces.

Additionally, the initial temperature of temperature for the main stove's components (still needed for steady-state modelling in FlowSimulation) was performed based on experimental results in Figure 10.

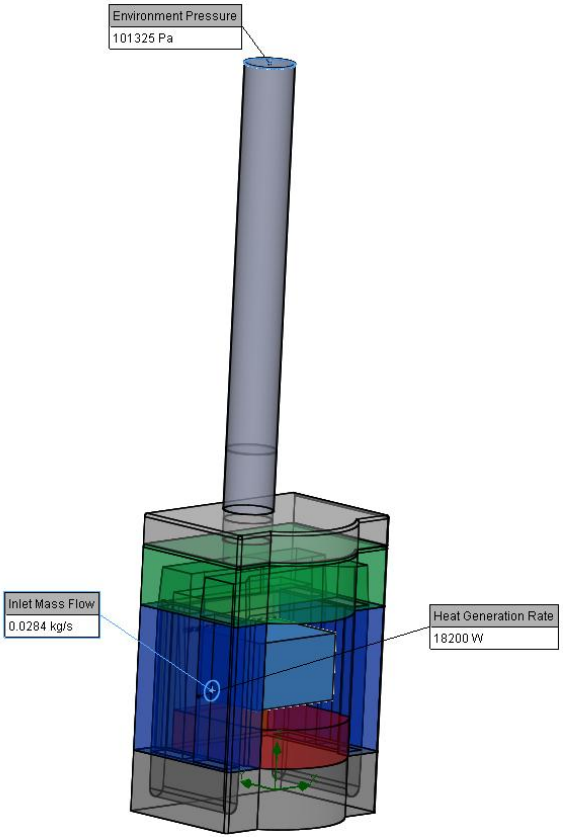

Figure 15 Specification of the sub-domain (stove) boundary conditions and heat generation rate

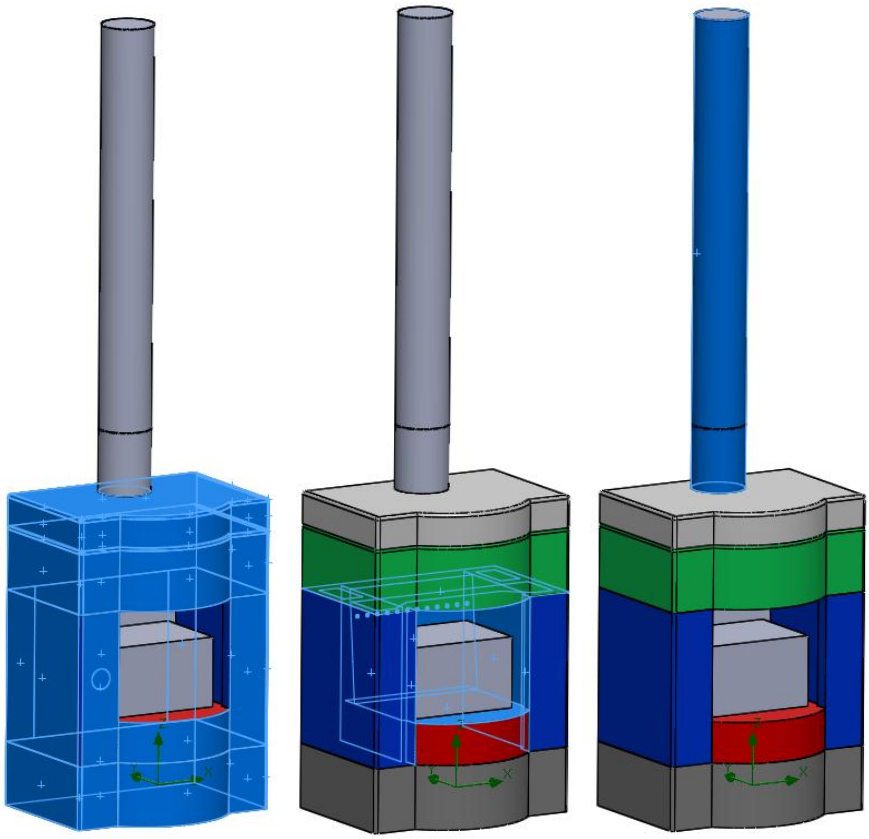

Figure 16 Radiative surfaces,(left) stove outer surfaces, (Middle) stove inner surfaces, (Right) stove exhaust pipe

The grid was generated for both the solid and fluid domains. The former was generated for all the solid parts including all the stove main components, glass door and exhaust pipe while for the latter the grid was generated for the fluid sub-domain inside the stove and also the main fluid domain (room). Number of mesh elements were increased while the temperature distribution was monitored across various components of stove for minimal variation for the purpose of the mesh independent analysis. Such study resulted in 786543 fluid elements and 423589 solid elements as shown in Figure 17.

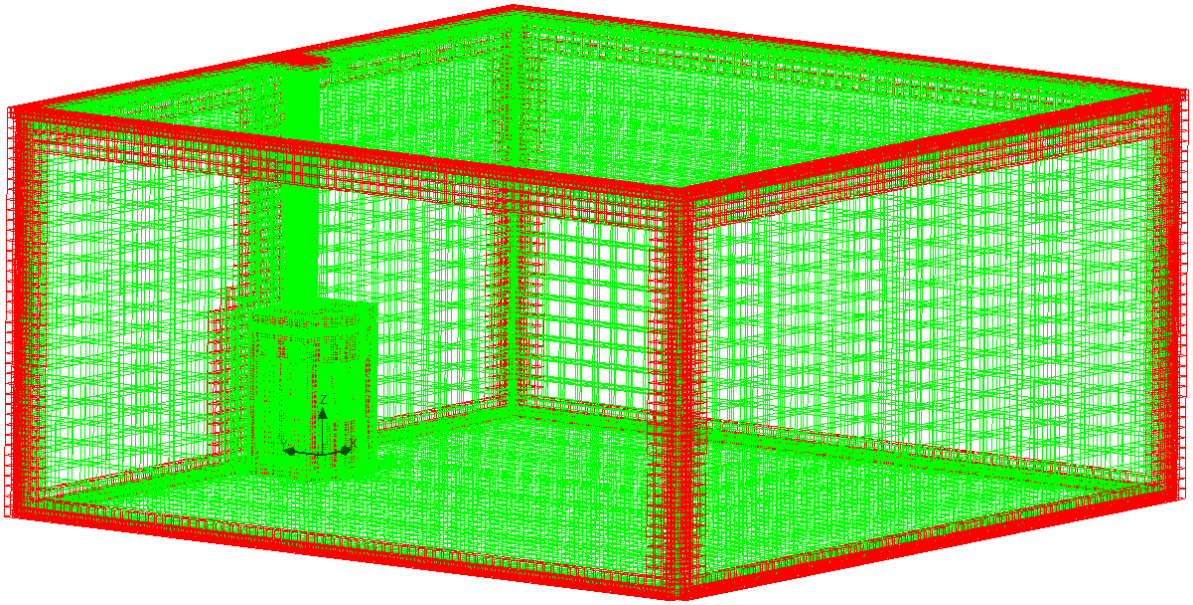

Figure 17 Generated grid for the numerical simulation of stove and room

5.2 Validation of the CFD model with the experimental results

The CFD model developed in SolidWorks FlowSimulation section 5.1 was initially validated with the results of burning 12.9kg of "Silver Birch" wood shown in Figure 6. The results were compared against the temperature distribution at various measurement points averaged over time (Table 4) and are presented in Figure 18. As it is clear, the CFD results are in fair agreement with the experimental values in all parts with the maximum deviation of 9% in the "Hotbox". It is only for the "Grate" part that the difference is larger with the value of 34.8%.

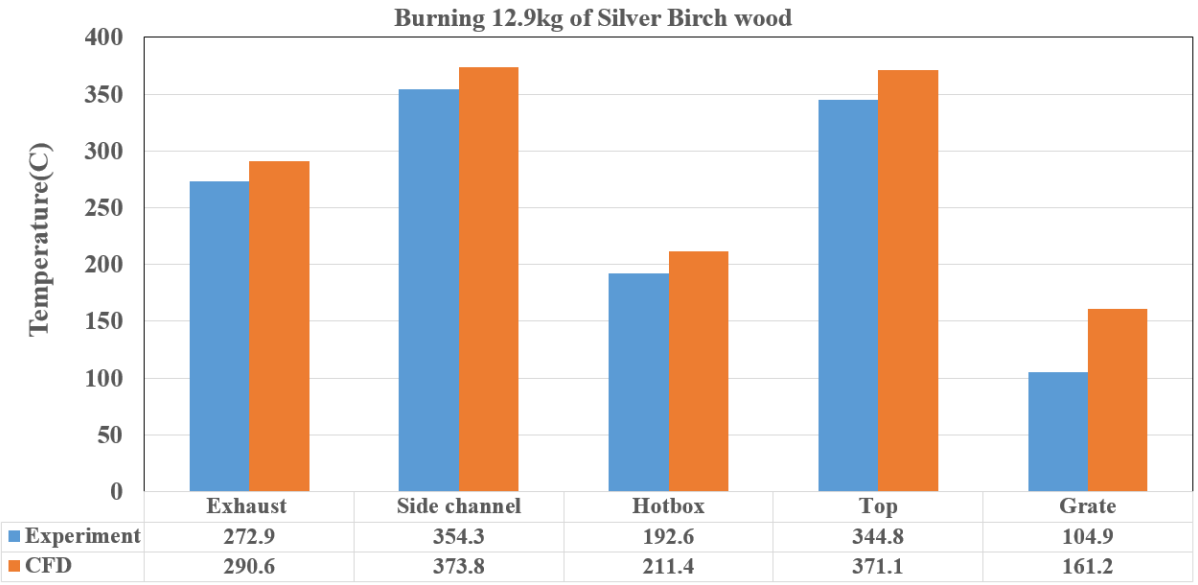

	Exhaust	Side channel	Hotbox	Top	Grate
Experiment	272.9	354.3	192.6	344.8	104.9
CFD	290.6	373.8	211.4	371.1	161.2

Figure 18 Comparison of the simulation results with experimental values for the temperature distribution at various parts of stove

This is due to the fact that in reality the majority combustion flames always travel upward (buoyancy effect) leading to lower temperature in the "Grate" part while for the CFD simulation the heat generation rate from the wood log block was released uniformly from all six faces leading to higher "Grate" temperature. Figures 19 and 20 illustrate the CFD results in terms of the temperature distribution cut plots across the room, the stove outer surface body temperature and temperature patterns inside the sub-domain (i.e. the stove).

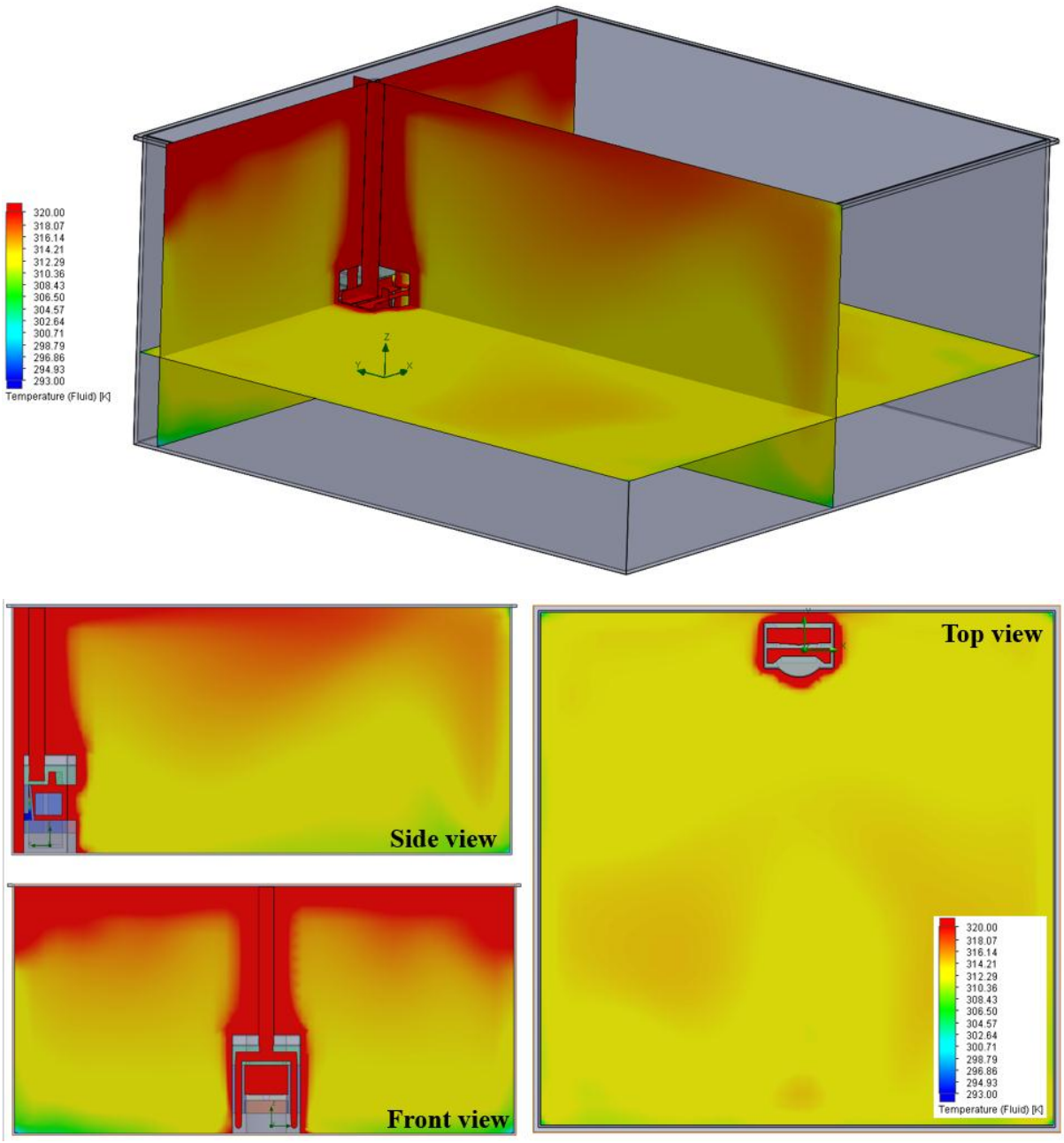

Figure 19 Temperature distribution across the room, (top) isometric view, (bottom) cut plots

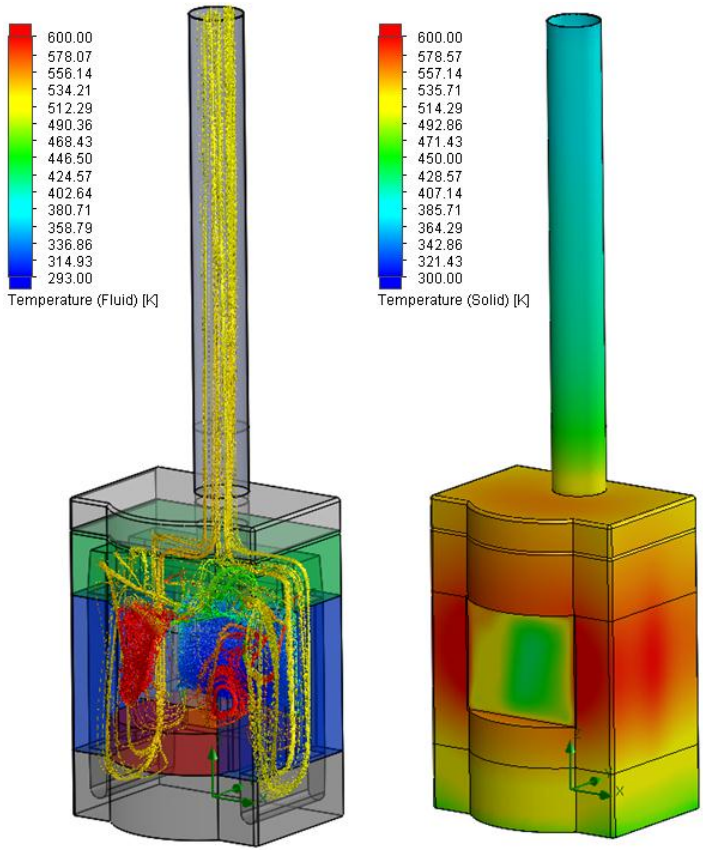

Figure 20 Temperature patterns inside the sub-domain (left), stove outer surface body temperature (right)

The model was employed to further validate the results of the closed loop water heating system described in section 4.2. In order to carry out such validation it was required to create another fluid sub-domain for the water inside the stainless steel coils. Figure 21 shows the fluid sub-domain created inside the model for simulating the water heating system integrated with the stove (Figure 9). The setup remained the same with the only difference that two extra boundary conditions as the water inlet flow rate and water exit pressure were specified for the water sub-domain with the water inlet temperature of 20 °C. The results of simulations are presented in Figure 22.

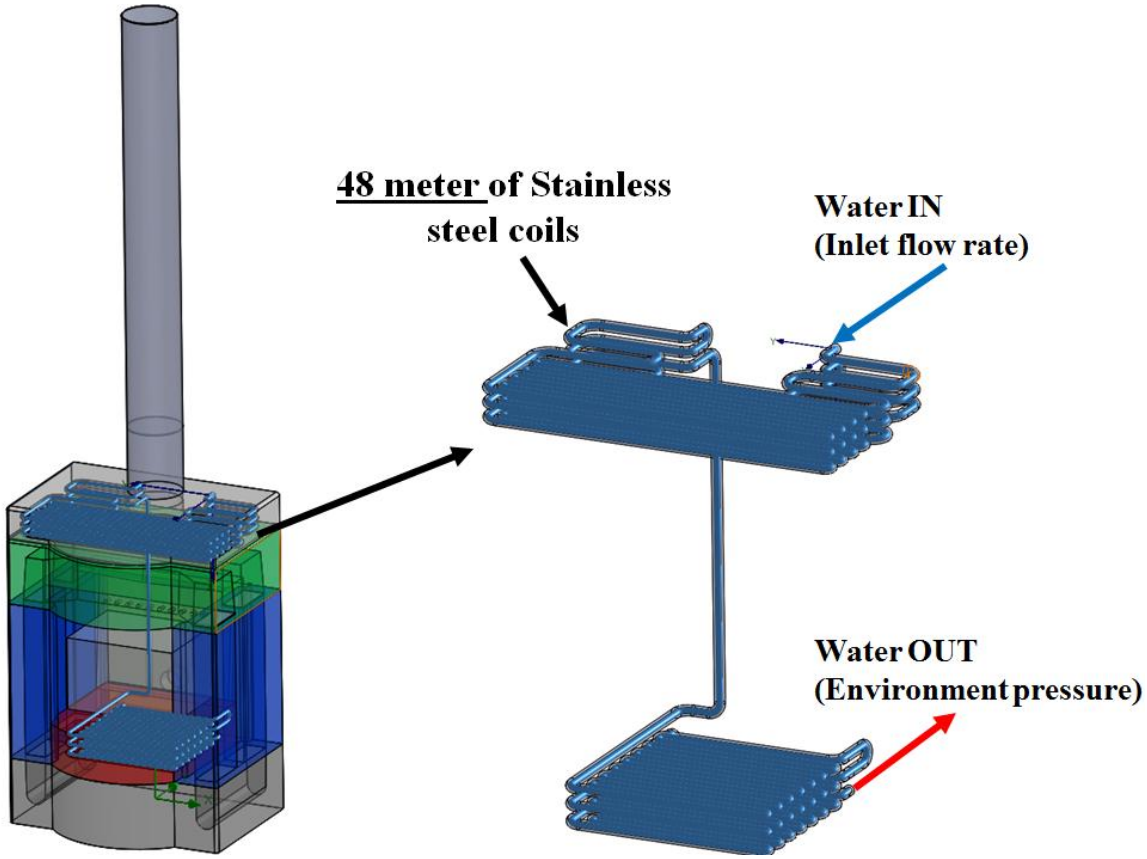

Figure 21 Sub-domain for the water heating system integrated in the “Hotbox” and “Grate”

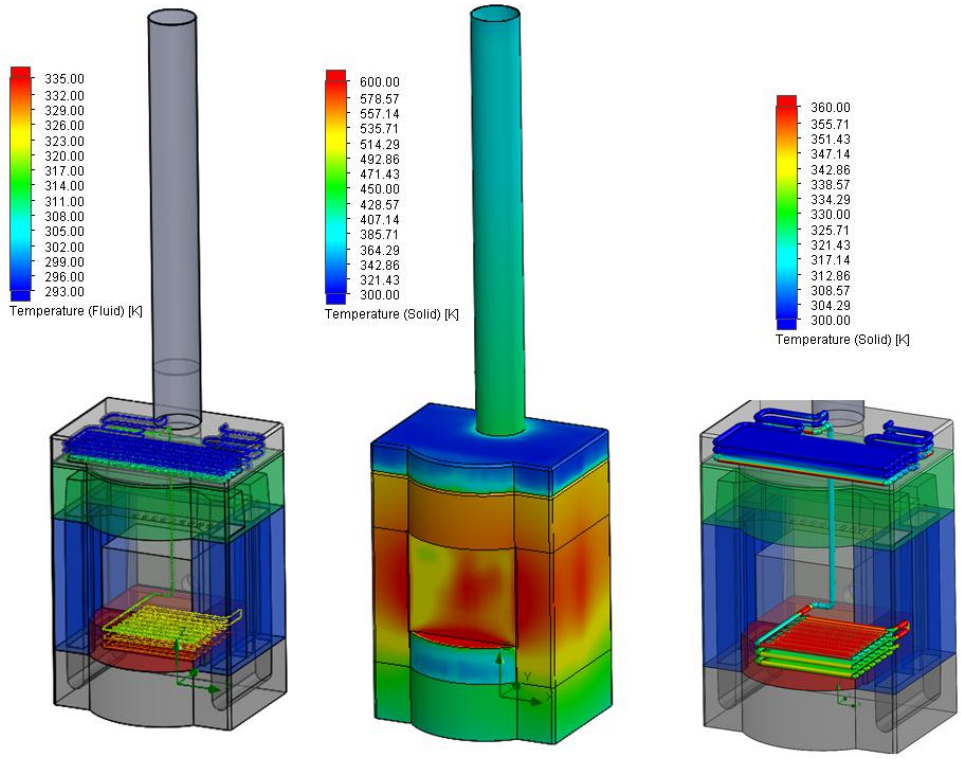

Figure 22 Simulation results for water heating system with coils integrated in “Hotbox” and “Grate”

As it is obvious from the results, implementation of the coils in the "Hotbox" and "Grate" led to lower temperature similar to the experimental values discussed in section 4.2. This lower temperature was observed in the experimental values obtained in section 4.2 when implementing the evaporator coils into the stove compared to the original configuration with no coils tested in section 4.1 and by comparing the values in Tables 4 and 5. Besides, comparing the stove outer solid temperature in Figure 22 with that of Figure 20 reveals that the Hotbox" and "Grate" solid temperature has reduced since the heat was captured by the water while increasing its temperature. Furthermore, the simulations provided the water inlet and exit temperatures from the ORC evaporator coils (Figure 21) and by employing Equation 4 the heat exposed on the stainless steel coils was obtained and compared with the experimental results (Figure 11) as shown in Figure 23.

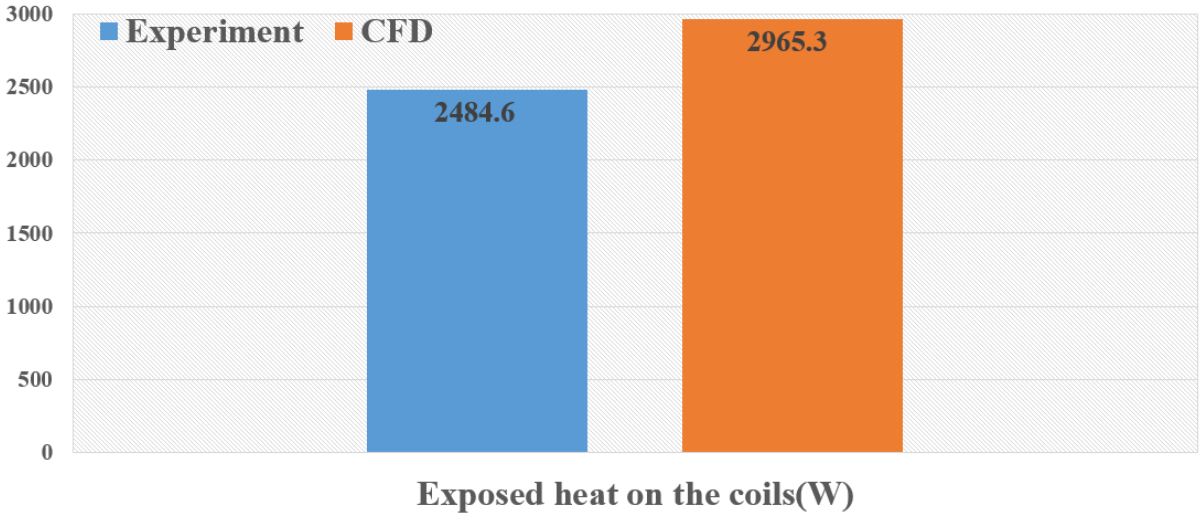

Figure 23 Comparison of the numerical and experimental results for the exposed heat on the stainless steel coils

As it is obvious from the results, the CFD value is in fair agreement with the experimental value with the former over-predicted the heat by about 16.2%. This over-prediction in the numerical results both for the temperature distribution and exposed heat shown in Figures 18 and 23 can be associated with the following factors:

1. The integration of the evaporator coils was fairly uniform in the "Hotbox" and "Grate" during CFD simulations which facilitated even exposure of the heat to the coils. But for the experiments it was not possible to implement the coils uniformly and they were fitted with no specific pattern in the "Hotbox" and "Grate" which resulted in relatively inefficient exposure of heat on the coils during experiments.

2. CFD simulations were conducted in a completely insulated room with no additional heat losses while the experiments were subjected to forced convection due to the possible room air velocity.

3. The combustion flames were dominantly travelling upward during experiments, while in the CFD simulations the heat was uniformly emitted from the wood log block from its all six sides leading to higher "Grate" temperature and consequently led to larger recovered heat during CFD analysis.

4. Exclusion of radiation produced by the actual flames from the combustion of the wood logs in the CFD simulation (due to the limitation of the software package used for this study and the need for more advanced and more complex simulation tools).

It should be mentioned that constant mass flow and heat release rates assumptions and all their important implications in the following sections are simple exploratory one that would need future work to establish gas mass flow rate based on equilibrium between the pressure drop caused by the flow and the hot gases buoyancy driving this flow, and is of course also linked to the fire heat release rate, which is also a function of the gas mass flow rate. Consequently, the CFD model can be assumed partially validated for the current design and operating conditions. Such model was employed to further investigate various WHR scenarios to increase the captured heat on the coils and thus increase the net electricity generation (Equation 1) as will be shown in section 5.3.

5.3 Further modifications for enhancing WHR using validated CFD model

The temperature values shown in Table 4 reveal that there exists substantial residual heat in the exhaust pipe with the average temperature of about 273 °C (or 290.7 °C from CFD) that is wasted to the surrounding environment. Therefore, such position has great potential to implement the ORC evaporator coils. By employing the validated CFD model (described in section 5.2) different scenarios were investigated by applying five different modifications to the coils. Such coils were implemented inside the exhaust pipe combined with the "Hotbox" in order to enhance the heat recovery and consequently increase the net electricity generation. Similar to section 5.2, the CFD setup remains the same with the associated boundary conditions for the water sub-domain. Figures 24 to 28 present the five different modifications that were investigated in this paper together with their CFD results. The difference between the "Modifications 1 and 2" is in the number of turns inside the exhaust pipe while having the same coil inner and outer diameter. Similarly, "Modifications 3 and 4" are also similar in terms of the coil size while having different number of turns. In fact, for "Modifications 2 and 4" the choice of the number of turns was so that the exhaust pipe was completely filled with coils for maximizing the heat transfer area. "Modification 5" was created similar to the "Modification 2" (same number of turns and coil size in the exhaust pipe) with the only difference that the coil was also extended to both "Side walls" (coils were located within the "Side walls" solid body).

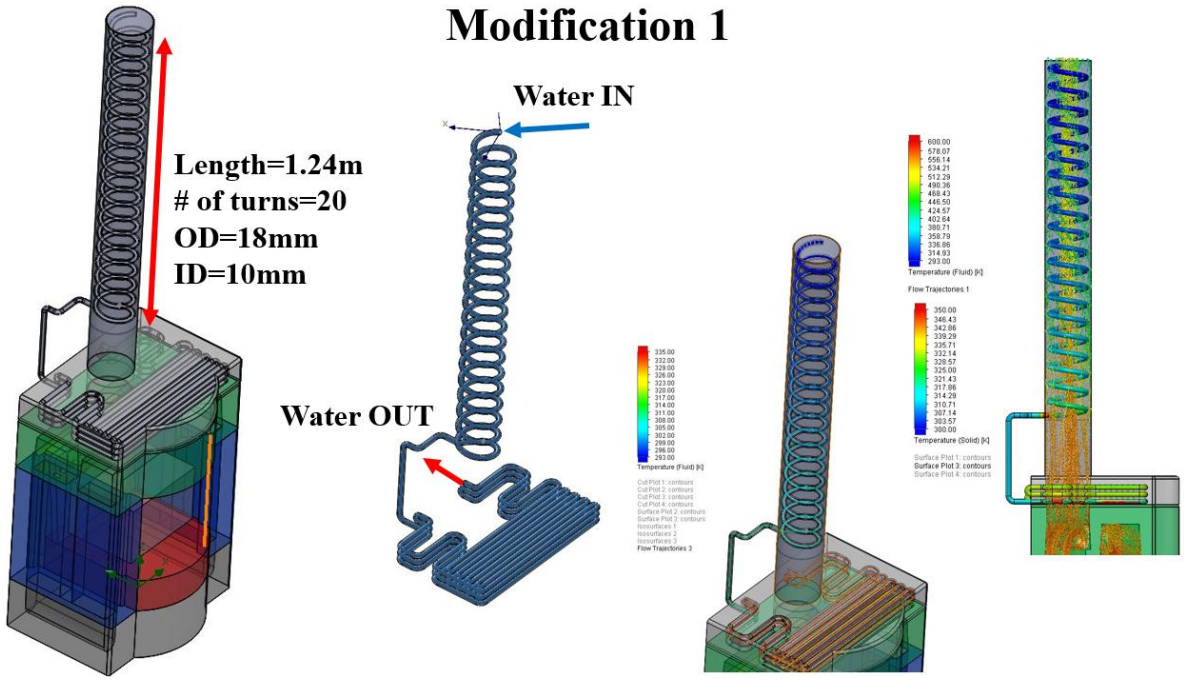

Figure 24 “Modification 1” geometry, water sub-domain and CFD results

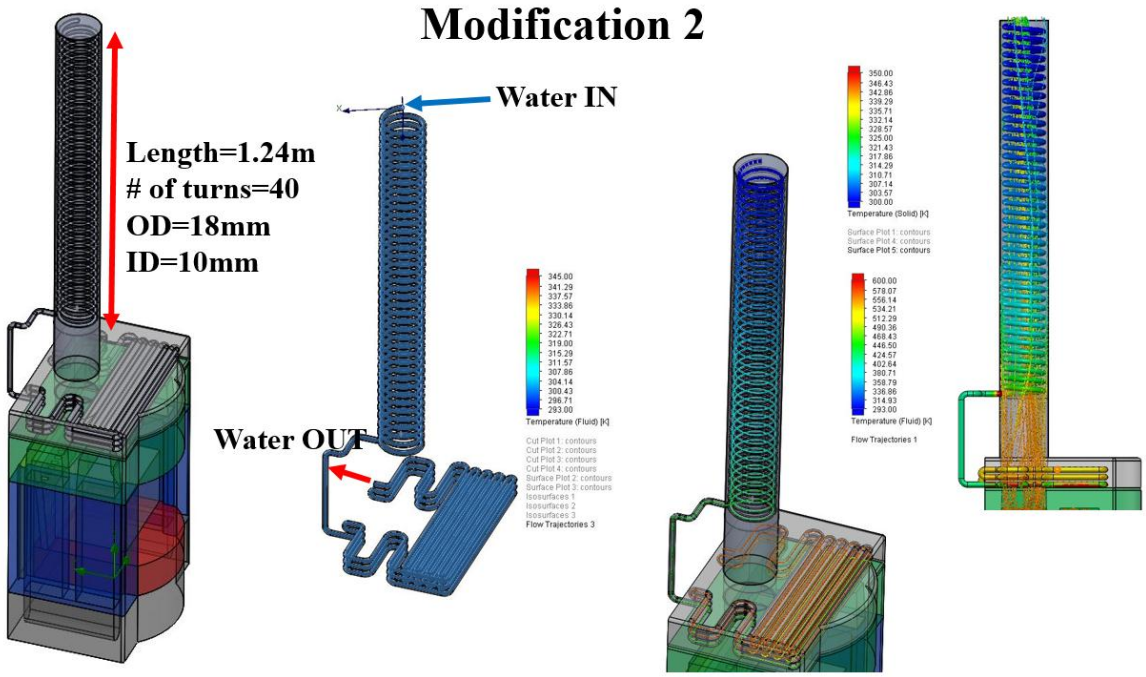

Figure 25 “Modification 2” geometry, water sub-domain and CFD results

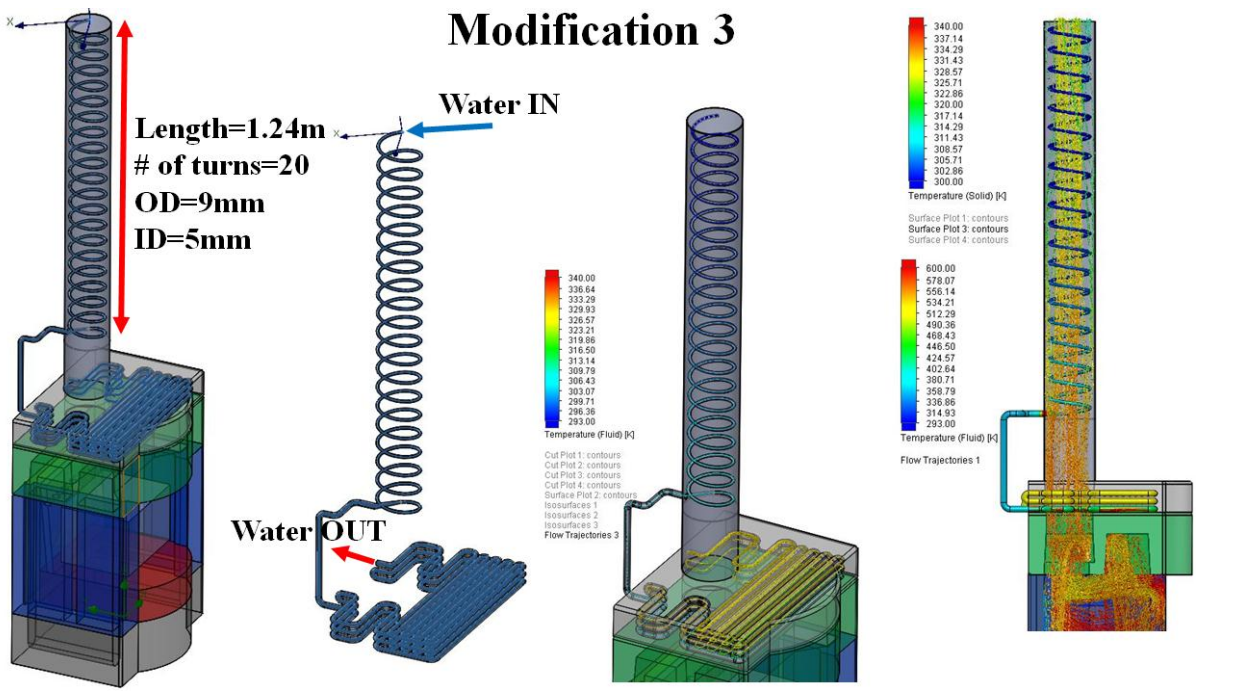

Figure 26 “Modification 3” geometry, water sub-domain and CFD results

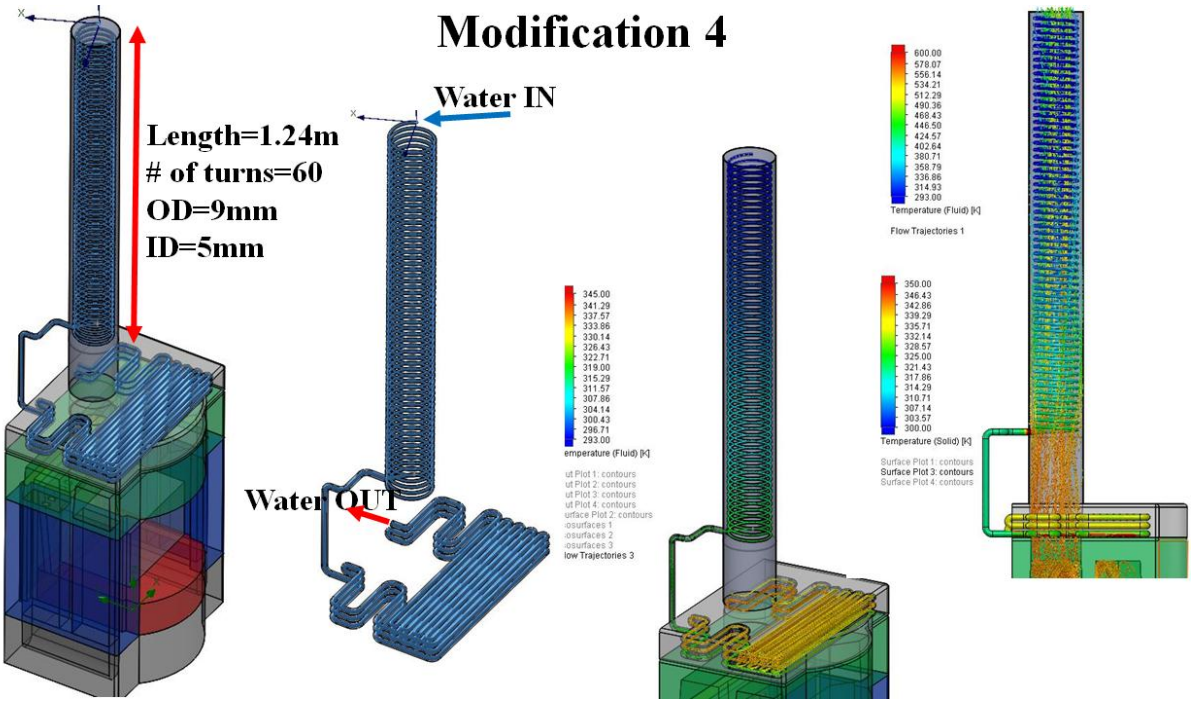

Figure 27 “Modification 4” geometry, water sub-domain and CFD results

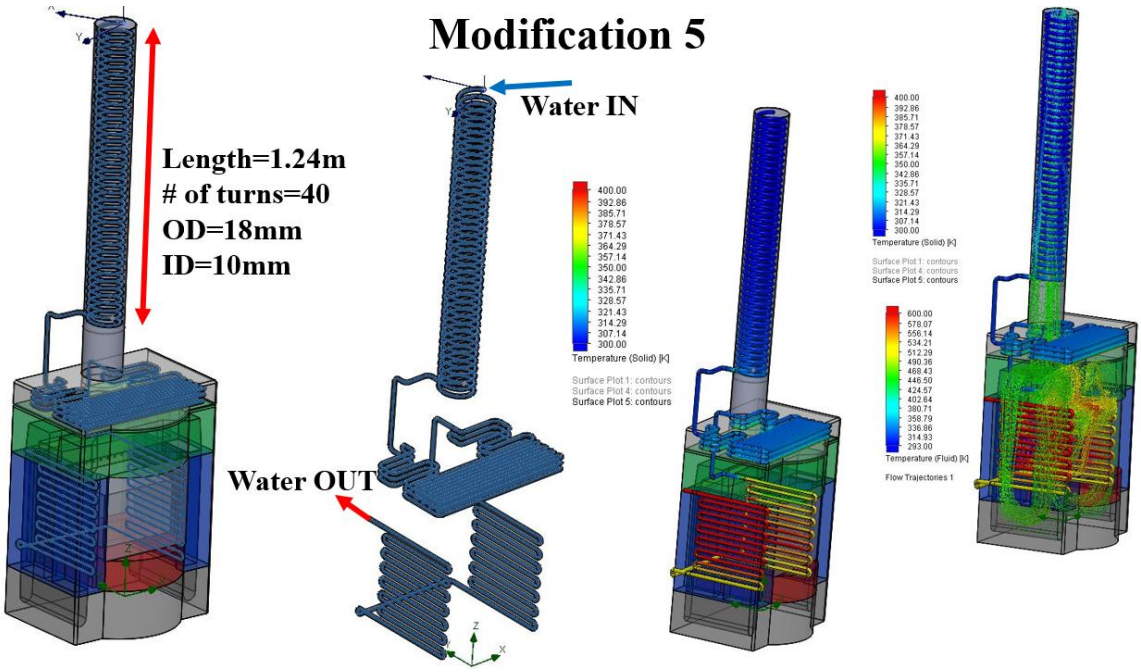

Figure 28 “Modification 5” geometry, water sub-domain and CFD results

Table 6 summarizes the main characteristics of all five configurations in terms of number of turns, total coil length and total heat transfer area.

Table 6 Summery of the main characteristics for the implemented modifications

Name	Number of turns (-)	Inner diameter (mm)	Outer diameter (mm)	Total coil length (m)	Total heat transfer area (m^2)
Modification 1	20	10	18	32.3	2.6
Modification 2	40	10	18	40.4	3.4
Modification 3	20	5	9	32.3	2.3
Modification 4	60	5	9	48.5	3
Modification 5	40	10	18	49.6	4.4

In order to assess the performance of each individual modifications in terms of heat recovery (captured heat on the coils), all the five configurations together with the original configuration (no coils) were compared in Figure 29. Based on the CFD results in Figure 18 for the original geometry (no coils), the flue gases enter the exhaust pipe at the high temperature of about 290 ˚C. Part of the heat was transferred to the surrounding while passing though the exhaust pipe and discharged to the environment at the temperature of about 261 ˚C. As it is evident in Figure 29, implementation of coils inside the exhaust pipe was advantageous in all

five modifications. Firstly, the temperature of flue gases entering the exhaust pipe was reduced due to the coils in the "Hotbox" and more importantly, part of the heat was recovered by the coils inside exhaust pipe leading to significantly lower temperatures at the exit of exhaust pipe compared to the original configuration. Among the investigated configurations, "Modifications 2, 4 and 5" are the most promising ones as they led to the lowest temperature levels at the exhaust. Employing Equation 4 together with the calculated water inlet and outlet temperatures, the recovered heat through the stainless steel coils was obtained as depicted in Figure 30. The maximum recovered heat of 13.6kW was obtained by "Modification 5" that has the lowest temperature of 95 ˚C at the exit of exhaust while "Modifications 2 and 4" recovered about 4.9kW and 4.8kW respectively.

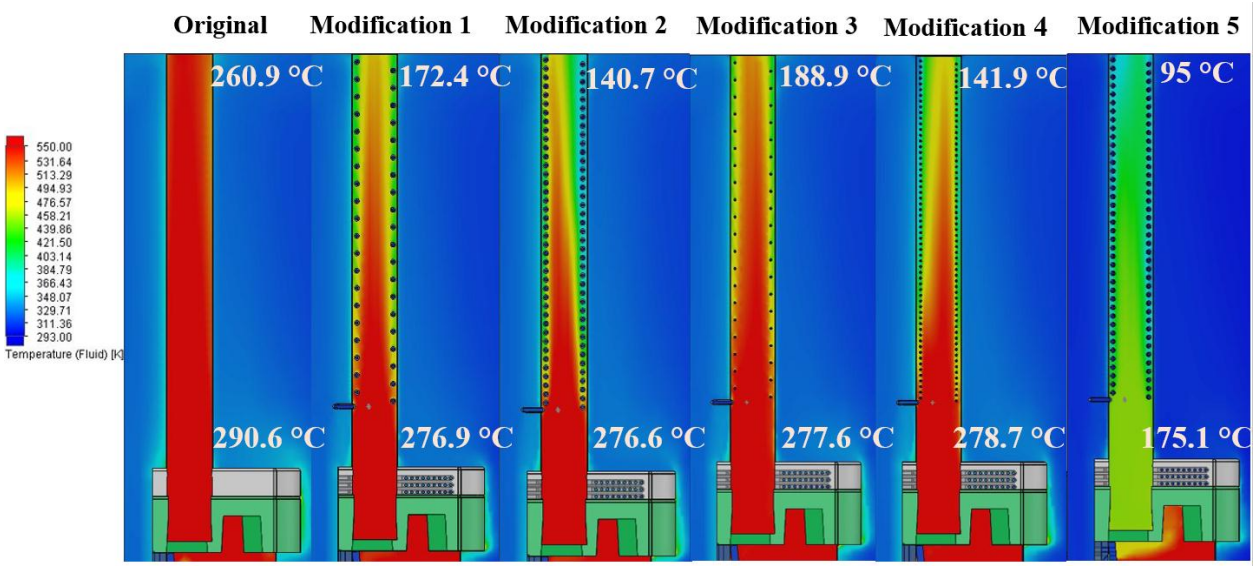

Figure 29 Comparison of the original configuration with five modifications in terms of temperature distribution in the exhaust pipe (water inlet temperature was specified to 20˚C in all cases)

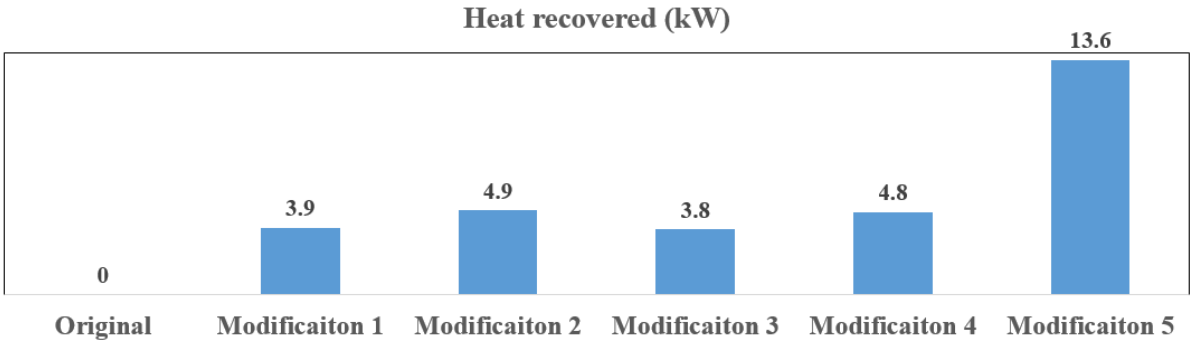

Figure 30 Recovered heat for all investigated modifications (water inlet temperature was specified to 20˚C in all cases)

The amount of heat loss through the exhaust was determined using Equation 5 assuming the environment temperature ($T_{environment}$) of 10 ˚C for a cold winter day in all cases.

$$Q_{heat\ loss} = \dot{m}_{air} C_{P,air} (T_{air@exit\ of\ exhaust\ pipe} - T_{environment}) \quad \text{Equation 5}$$

Figure 31 presents the heat loss to the environment for all five modifications together with the original configuration. Obviously the largest heat loss was obtained by the original configuration that has no coils for recovering the heat. On the other hand, the minimum heat loss is achieved by the "Modification 5" that exhibited the largest recovered heat as was shown in Figure 30 followed by "Modifications 2 and 4".

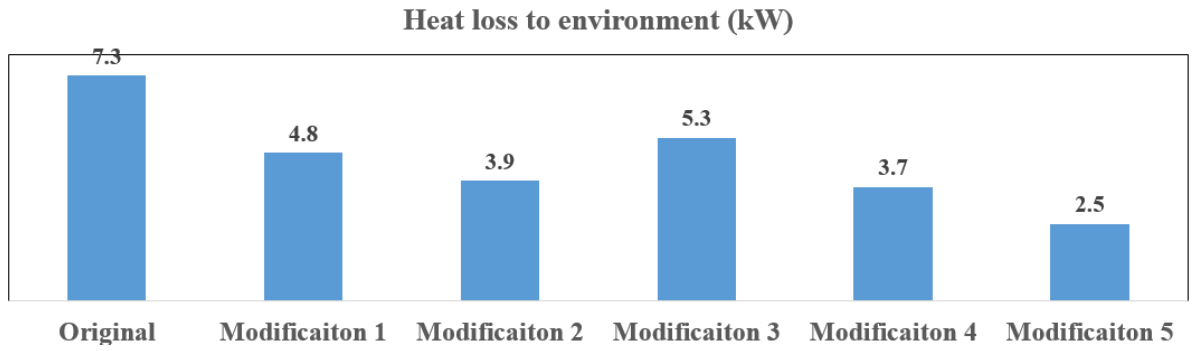

Figure 31 Heat loss to the environment for all five modifications (environment temperature was specified to 10˚C in all cases)

Following the same procedure as in section 4.2, the maximum obtainable ORC thermal efficiency ($\eta_{thermal,ORC}$) can be calculated with the known heat source inlet and exit temperatures for all the five modifications. The heat source inlet temperature ($T_{hs,in}$) was obtained as the

average of the exhaust pipe and "Hotbox" temperatures before implementing the evaporator coils (i.e. from the original geometry) with the value of 254.3 °C. The heat source exit temperature ($T_{hs,out}$) was obtained for each modification individually after implementing the evaporator coils by averaging the temperature in the exhaust pipe and "Hotbox" parts. Since the value of $T_{hs,in}$ was greater than 180 °C, Equation 2-b was employed for calculating the $\eta_{thermal,ORC}$ and the results are summarized in Table 7. Consequently, with the calculated ORC heat input (Q_{in}) as shown in Figure 30 and the $\eta_{thermal,ORC}$ obtained from Table 7 the net power output (W_{net}) from the ORC system was determined using Equation 1 and the results are summarized in Table 7.

Table 7 Maximum obtainable ORC thermal efficiency for all investigated modifications

Configuration	Heat source inlet temperature [°C]	Heat source outlet temperature [°C]	Maximum ORC thermal efficiency [%]	ORC net power output [W]
Modification 1	254.3	180.9	23.2	923.4
Modification 2	254.3	171.7	22.9	1113.7
Modification 3	254.3	186.2	23.3	879.8
Modification 4	254.3	167	22.8	1088.7
Modification 5	254.3	110	20.8	2833.8

The maximum power output of 2.8kW was achieved with the "Modification 5" since such configuration recovered the largest heat by the evaporator coils with minimal heat losses to the environment. The results in Table 7 are significantly higher than the previous value of 358W obtained by the evaporator in the "Hotbox" and "Grate" parts (section 4.2) and highlight the potential of the proposed modifications to increase the electricity generation from the waste heat of the stove. The stove energy conversion efficiency was obtained using Equation 6.

$$\eta_{\text{stove}} = \frac{\text{Useful output}}{\text{Total heat input}} = \frac{\text{Total heat input} - \text{Heat loss to environment}}{\text{Total heat input}} \quad \text{Equation 6}$$

The "total heat input" is the total heat release by the biomass fuel (Silver Birch wood logs) while the "useful output" is the amount of heat that was used directly for space heating and indirectly for electricity generation through the ORC system. The "total heat input" was about

18.2kW as explained in section 5.1 while “useful heat output” was obtained by the subtraction of the “heat loss to the environment” (Figure 31) from the “total heat input”. Figure 32 depicts the stove energy conversion efficiency for the original configuration as well as for all of the proposed modifications.

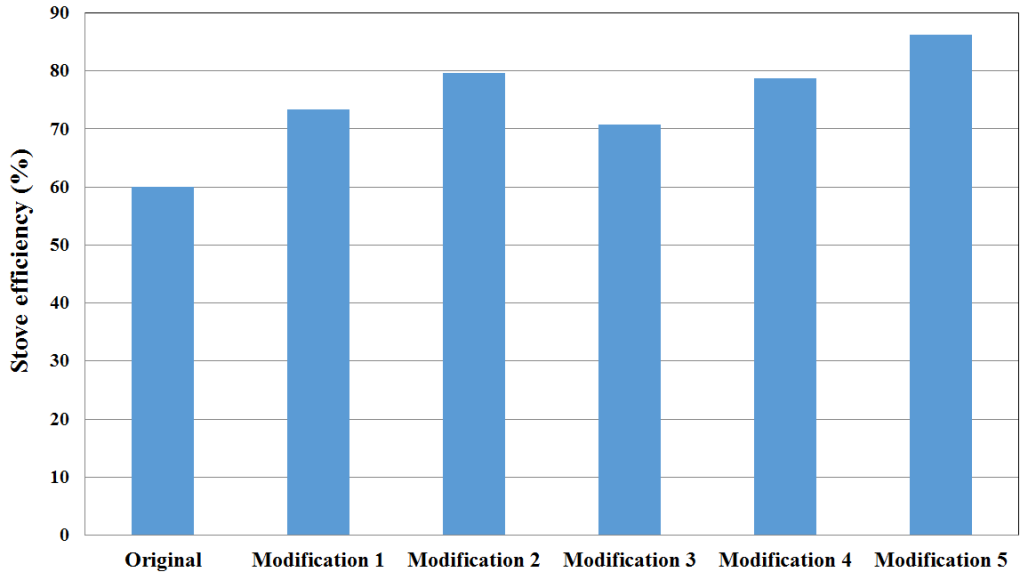

Figure 32 Stove energy conversion efficiency for original configuration as well as for proposed modifications

It is evident that all the imposed modifications substantially improved the stove’s efficiency with the maximum value of about 25% obtained by “Modification 5” followed by “Modification 2” with the efficiency improvement of about 20%. Such results underline the effectiveness and potential of the proposed modification to further improve the stove’s performance.

It is crucial to evaluate the effect of investigated modifications on the heating functionality of the stove (which is its main purpose) to ensure such modifications are not detrimental to its heating performance. Therefore, for the simulated room in which the stove was located (Figure 14), the room average temperature was obtained for all five modifications together with the original configuration as depicted in Figure 33. As it is obvious for “Modifications 1 to 4” the

room temperatures were in close proximity with the original configuration and reveal that such cases did not significantly affect the heating performance of the stove while producing electricity (Table 7). However, there was substantial reduction in the room temperature for the "Modification 5" compared to the original configuration which underlines that such modification had substantially affected the heating performance of the stove, though, it recovered the largest amount heat. This feature is highlighted by comparing the stove outer surface solid temperature for "Modifications 2 and 5" as illustrated in Figure 34. As it is clear, for the latter the stove solid temperature is considerably lower and the stove was not capable of heating the room as required. This was due to the fact that the majority of heat was captured by the coils implemented in the "Side walls" of the combustion chamber prior it could be transferred to the surrounding via convection and radiation. Therefore, "Modification 5" failed to preserve the heating functionality of the stove, though, it produced the largest power.

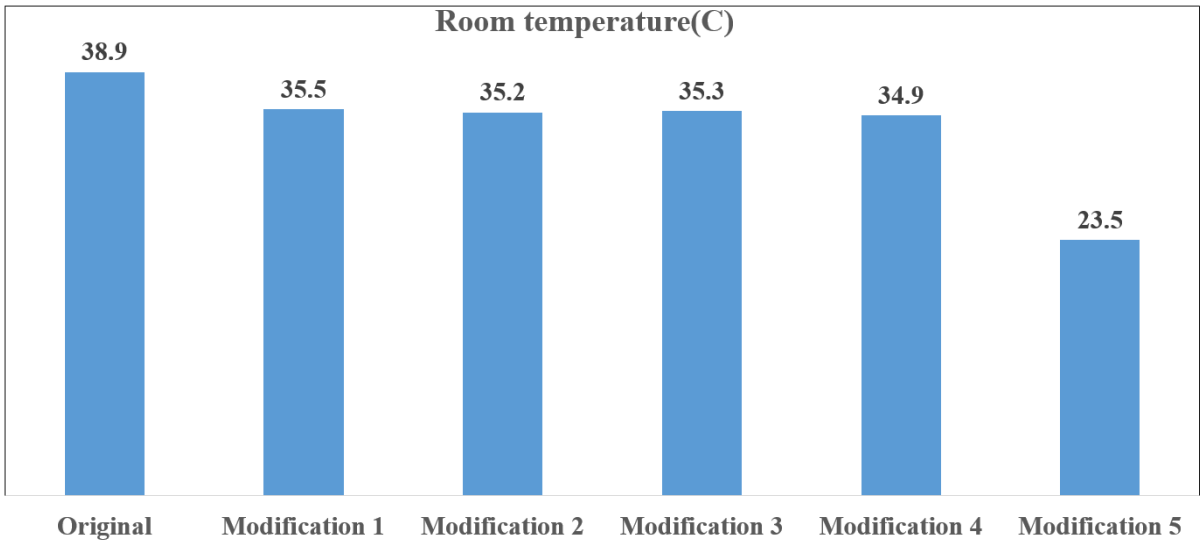

Figure 33 Average room temperature for all modifications (the room initial temperature was specified to 10 ˚C in all cases)

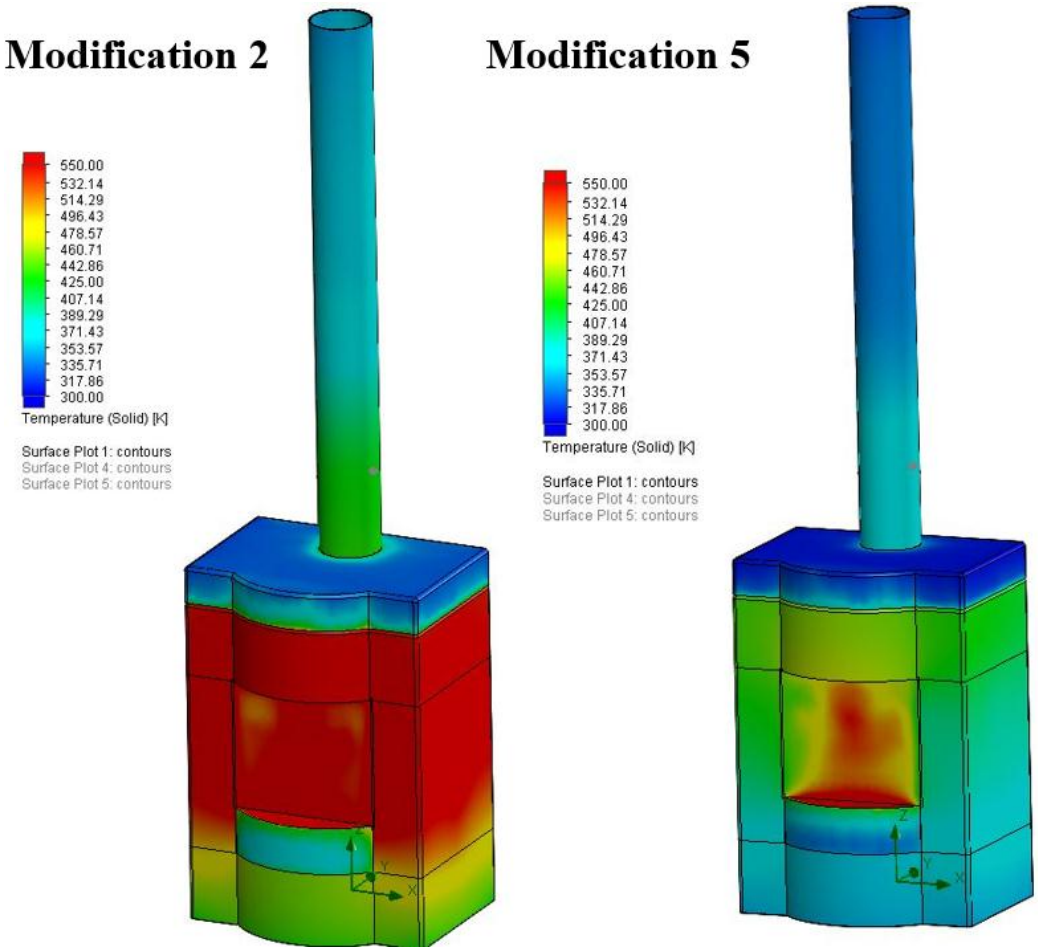

Figure 34 Comparison of the stove outer surface solid temperature for "Modifications 2 and 5"

As shown in Figure 33 the room temperature was considerably higher than the thermal comfort zone for the original configuration as well as "Modifications 1 to 4". This was due to the fact that all the CFD simulations were conducted in a room with the dimensions shown in Figure 14. Such dimensions were almost similar to the room in which all the experiments were conducted (section 4) for the purpose of comparison.

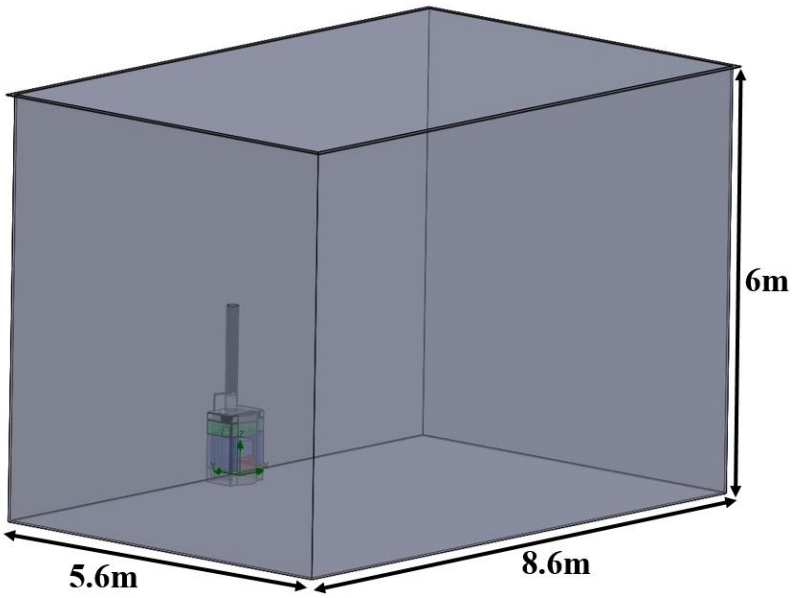

Figure 35 Standard two-storey house dimensions

As mentioned in section 3, the stove model under investigation was designed for space heating of a two –storey four-bedroom house. Therefore, for the most promising cases ("Modifications 2 and 5") that generated the largest electricity (Table 7) the numerical simulations were re-conducted but instead of simulating the stove in the room with dimensions shown in Figure 14, the stove was located in a significantly larger room with the standard dimensions of a typical two-storey house (Figure 35) and the results are presented in Figures 36 and 37. Figure 36 shows that even by implementing the heating coils inside the "Hotbox" and exhaust pipe (Modification 2), the heating performance of the stove was not significantly affected as the achieved room temperature was in good agreement with the stove performance characteristics according to the manufacturer [8] and also close to the desired temperature range of 21 to 23˚C. In contrast, it is obvious from the results in Figure 37 that the room temperature was significantly below this range when employing "Modification 5". Therefore, implementation of such configuration should be limited to smaller houses (probably one-storey two-bedroom) and requires further investigations.

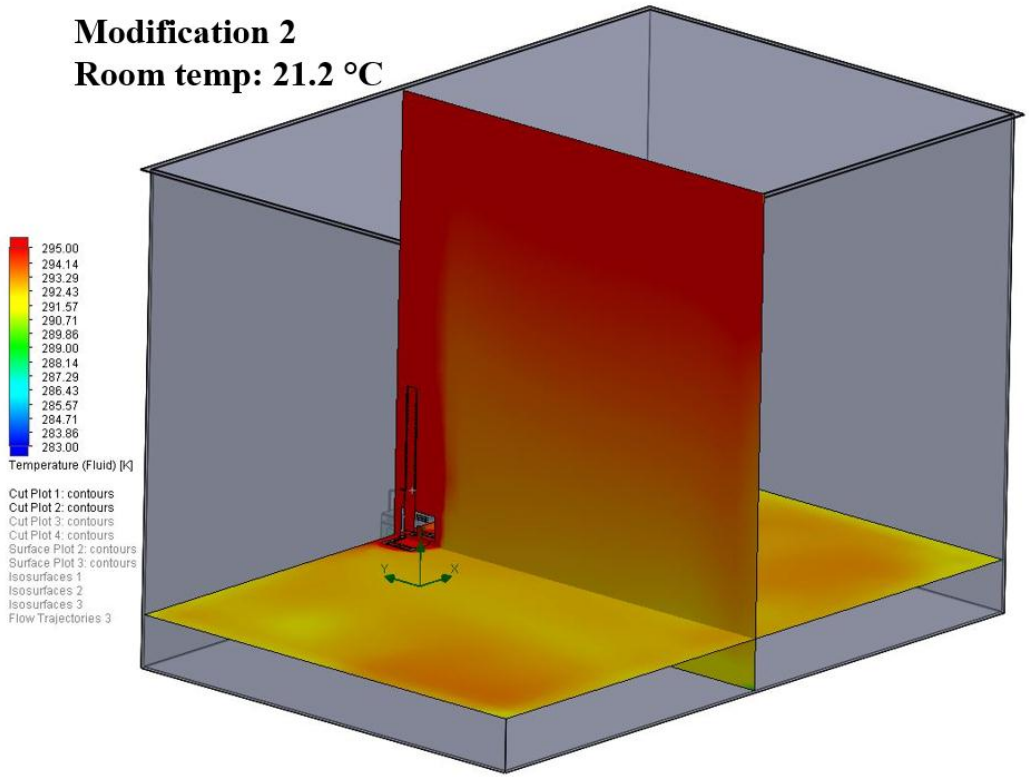

Figure 36 Temperature distribution cut plots and average room temperature for "Modification 2" simulated in a two-storey room (initial room temperature was 10˚C)

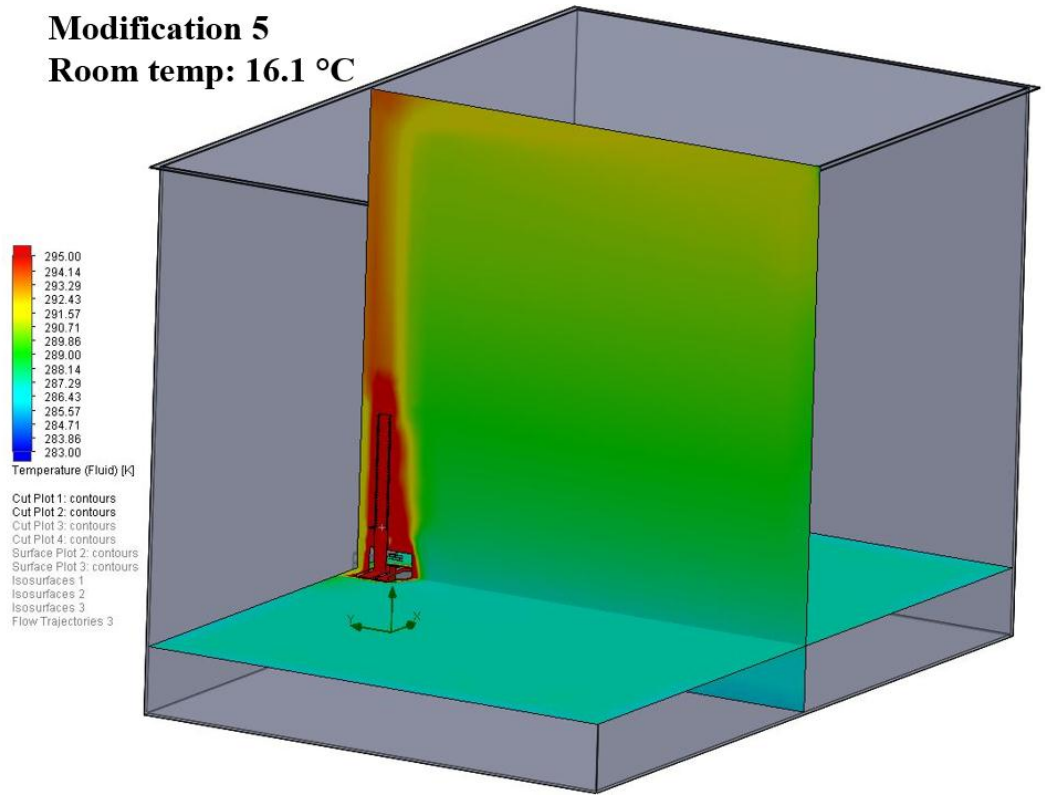

Figure 37 Temperature distribution cut plots and average room temperature for "Modification 5" simulated in two-storey room (initial room temperature was 10˚C)

6. Future work

Although this study is a pioneering one for use of CFD modelling for this kind of applications, it is still in early developments and needs further investigation of other facets as listed below:

- Investigation of change in component concentration of harmful/flue gases and deterioration due to moisture problems due to the change in temperature of the exhaust pipe by inclusion of ORC evaporator coils.
- Calculation of the gas mass flow rate using CFD based on the equilibrium between the pressure drop caused by the flow and the hot gases buoyancy driving this flow, and fire heat release rate to extend the applicability of this methodology to other designs and configurations.

7. Conclusions

This paper aimed at investigating the feasibility of electricity generation using the ORC technology through the Waste Heat Recovery of a biomass (wood log) stove available commercially. Despite the good performance of this stove, there was still significant amount of heat that was wasted through the exhaust at the temperature range of between 240 $^{\circ}$C to 270 $^{\circ}$C. At such temperature levels the amount of the waste heat was about 40% of the total energy release by the biomass fuel. Therefore, both experimental testing and CFD simulations were performed to enhance the performance of the stove by introducing a WHR system that can be integrated within the stove. Experimental testing of the stove showed that there were several potential positions with high temperature that can be employed for installation of the ORC evaporator (heating coils) for collecting the waste heat. Among the investigated positions the "Side walls" interior channels and the "Top" part exhibited the highest temperature, however, implementation of the ORC evaporator in such positions proved to introduce additional complexities and cost to the system. It was shown that with minimal alteration of the stove and

at low cost it was possible to install the ORC evaporator coils in the "Hotbox" and "Grate" parts combined to measure the captured heat by the heating coils using a closed loop water heating system. It was estimated that 357.7W of electricity can be generated if the ORC evaporator be implemented in the "Hotbox" and "Grate" and the stove's efficiency improvement of about 14% while reducing the heat losses from about 40% to 26.3%. Numerical modelling of the stove using the FlowSimulation CFD software showed that, the CFD model can accurately predict the temperature distribution across the stove as well as predicting the recovered heat when comparing the results with the experiments. Moreover, the CFD model showed that it was possible to considerably enhance the WHR by implementing the ORC evaporator coils inside the "Side walls", exhaust pipe and the "Hotbox" parts (Modification 5). Among the investigated scenarios using the validated CFD model, "Modification 5" showed that the heat loss to the environment can be reduced to about 14% of the total energy input (burned biomass fuel) compared the original case with the heat loss of about 40%. Such configuration improves the stove efficiency by about 25% with the maximum electricity generation of 2.8kW. However, it was also shown that such configuration (Modification 5) can remarkably affect the heating functionality of the stove as the room temperature dropped about 6 °C below the thermal comfort temperature of 23 °C. To preserve both the heating functionality as well as improving the stove's efficiency, "Modification 2" was found to be the most effective as it not only improved the efficiency by about 20% with electricity generation of 1.1kW but also kept room temperature only about 2 °C below the desired temperature of 23 °C. Such results highlight the benefits of the present study to further improve the performance of the investigated biomass stove and its potential for DPG systems.

7. Acknowledgement

The authors gratefully acknowledge the financial support by the European Regional Development Fund for Accelerating Business-knowledge Base Innovation Activity (ABIA) project.

References

1. International Energy Agency, I., *Energy Technology Perspectives−ETP2014, Harnessing electricity's potential* 2014.
2. World Energy Council *World Energy Perspective- Energy Efficiency Technologies*. 2013.
3. Ackermann, T., G. Andersson, and L. Söder, *Distributed generation: a definition.* Electric Power Systems Research, 2001. **57**(3): p. 195-204.
4. Siemens power generation division, *Waste heat recovery with organic Rankine cycle technology - http://www.energy.siemens.com/mx/pool/hq/power-generation/steam-turbines/downloads/brochure-orc-organic-rankine-cycle-technology_EN.pdf.* 2014.
5. IEA, I.E.A., *Key world energy statistics*. 2008.
6. Rahbar, K., S. Mahmoud, and R. Al-Dadah, *Mean-line modeling and CFD analysis of a miniature radial turbine for distributed power generation systems.* International Journal of Low-Carbon Technologies:doi: 10.1093/ijlct/ctu028, 2014.
7. ECCO stove. 2015 18/02/2015]; Available from: http://www.landyvent.co.uk/#!ecco-stove/x2hnx.
8. ECCO stove. 2014 18/02/2015]; Available from: http://www.eccostove.com/home.
9. Dixon, T.F., et al., *Development of advanced technology for biomass combustion—CFD as an essential tool.* Fuel, 2005. **84**(10): p. 1303-1311.
10. Ravi, M.R., S. Kohli, and A. Ray, *Use of CFD simulation as a design tool for biomass stoves.* Energy for Sustainable Development, 2002. **6**(2): p. 20-27.
11. Scharler, R., et al. *CFD simulations as efficient tool for the development and opimization of small-scale biomass furnaces and stoves* in *19th European Biomass conference and exhibition* 2011. Berline, Germany
12. Macqueron, C. *Computational Fluid Dynamics Modeling of a wood-burning stove-heated sauna using NIST's Fire Dynamics Simulator*. 2014.
13. Scharler, R., et al. *CFD based design and optimization of wood log fired stoves* in *17th European Biomass conference and exhibition, From research to industry and markets* 2009. 29June- 03 July Hamburg, Germany.
14. Rahbar, K., *Development and optimization of small-scale radial inflow turbine for waste heat recovery with organic rankine cycle*, in *School of Mechanical Engineering*. 2016, University of Birmingham: College of Engineering & Physical Sciences.
15. Rahbar, K., et al., *Parametric analysis and optimization of a small-scale radial turbine for Organic Rankine Cycle.* Energy, 2015 [a]. **83**(0): p. 696-711.
16. Rahbar, K., et al., *Modelling and optimization of organic Rankine cycle based on a small-scale radial inflow turbine.* Energy Conversion and Management, 2015 [b]. **91**(0): p. 186-198.
17. Quoilin, S., et al., *Techno-economic survey of Organic Rankine Cycle (ORC) systems.* Renewable and Sustainable Energy Reviews, 2013. **22**: p. 168-186.
18. Larsen, U., et al., *Multiple regression models for the prediction of the maximum obtainable thermal efficiency of organic Rankine cycles.* Energy, 2014. **65**(0): p. 503-510.
19. stove, E. *ECCO stove model E-678 technical description*. [cited 2016; Available from: http://eccostove.com/models/e678.
20. UK, L.V. *Ecco Stove performance evaluation*. 2015 [cited 2016; Available from: http://eccostove.com/sites/1/media/files/Ecco%20Stove%20performance%20evaluation.pdf.

21. Omega. *TJ Thermocouple Series* 2017 [cited 2017 22]; Available from: http://www.omega.co.uk/pptst/TJ36-ICIN.html.
22. Technology, P. *Technical specifications* 2017 [cited 2017 22]; Available from: https://www.picotech.com/data-logger/tc-08/thermocouple-data-logger.
23. MatWeb. *Silver Birch Wood Specification* 2017 [cited 2017 22]; Available from: http://www.matweb.com/search/datasheet.aspx?matguid=c499c231f20d4284a4da8bea3d2644fc&n=1&ckck=1.
24. Ltd, I. *Circulation Pumps for Central Heating* 2017 [cited 2017 23]; Available from: http://www.interpartspares.co.uk/929.htm.
25. Futurlec. *Futurlec DigiFlow Flow Meter with Flow Sensor*. 2017; Available from: http://www.futurlec.com/Flow_Sensor.shtml.
26. Solidworks. *Soliworks Flow Simulation 2012 Technical Reference* 2014 [cited 2017 23]; Available from: https://d2t1xqejof9utc.cloudfront.net/files/18565/SW_CFD_technical_reference.pdf?1361897013.
27. ROBAX, S. *SCHOTT ROBAX PROPERTIES* 2017 [cited 2017 23]; Available from: http://www.schott.com/hometech/english/products/robax/.
28. Incropera, F.P., *Fundamentals of Heat and Mass Transfer*. 2006: John Wiley \& Sons.

Nomenclature

Symbols

A	Area [m^2]
C_p	specific heat capacity [J/kg-K]
$\dot{m}$	Mass flow rate [kg/s]
Q	Heat [W]
T	Temperature [K] and [°C] for Equation 2
V	Velocity [m/s]
W	Power output [W]

Greek letters

η	Efficiency [%]
ρ	Density [kg/m^3]

Subscripts

1 to 7	Positions across the stove
c	Condenser
exp	Expander
hs	Heat source
in	Input, inlet
out	Output, outlet
pp	Pinch point temperature difference

Acronyms

IEA	International Energy Agency
CFD	Computational Fluid Dynamics
CHP	Combined Heat and Power
CPG	Centralized Power Generation
DPG	Distributed Power Generation
EES	Engineering Equation Solver

FDS	Fire Dynamics Simulator
ORC	Organic Rankine Cycle
SRC	Steam Rankine Cycle
WHR	Waste Heat Recovery

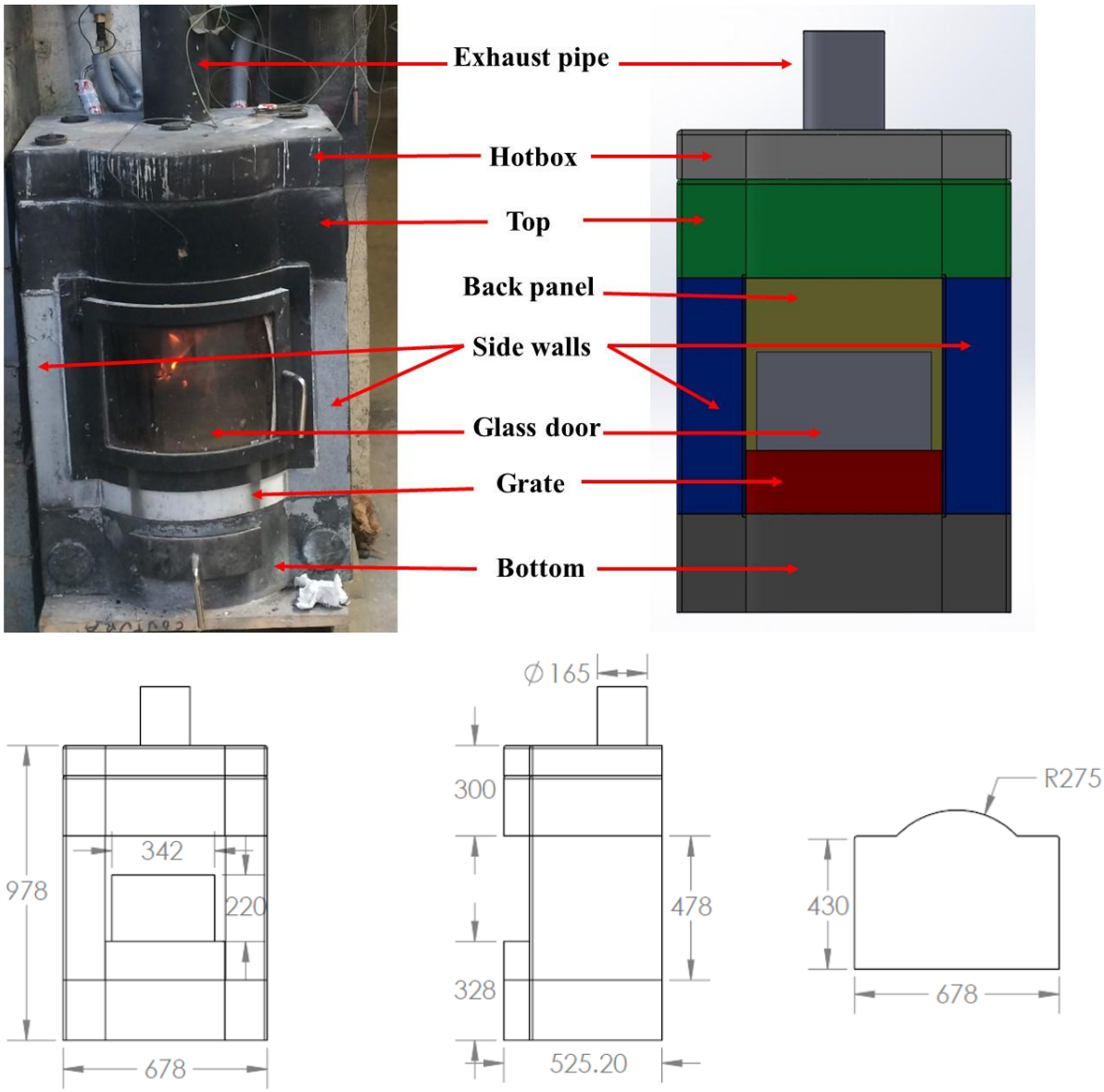

Figure 3. Biomass stove components, (Top-left) manufactured, (Top-right) 3-D CAD model, (Bottom) Stove dimensions in millimetre